Posted on 30 Nov 2022 — CC-BY-NC 4 — https://doi.org/10.1002/essoar.10505711/v2 — This a preprint and has not been peer reviewed. Data may be preliminary.

Carbon cycle response to temperature overshoot beyond 2 °C – an analysis of CMIP6 models

Irina Melnikova[1,1], Olivier Boucher[1,1], Patricia Cadule[2,2], Philippe Ciais[3,3], Thomas Gasser[4,4], Yann Quilcaille[4,4], Hideo Shiogama[5,5], Kaoru Tachiiri[6,6], Tokuta Yokohata[5,5], and Katsumasa Tanaka[7,7]

[1]Institut Pierre-Simon Laplace
[2]Institut Pierre-Simon Laplace, Sorbonne Université / CNRS
[3]Laboratory for Climate Sciences and the Environment (LSCE)
[4]International Institute for Applied Systems Analysis (IIASA)
[5]National Institute for Environmental Studies
[6]Japan Agency for Marine-Earth Science and Technology
[7]CEA Saclay,National Institute for Environmental Studies (NIES)

November 30, 2022

Abstract

There is a substantial gap between the current emissions of greenhouse gases and levels required for achieving the 2 and 1.5 °C temperature targets of the Paris Agreement. Understanding the implications of a temperature overshoot is thus an increasingly relevant research topic. Here we explore the carbon cycle feedbacks over land and ocean in the SSP5-3.4-OS overshoot scenario by using an ensemble of Coupled Model Intercomparison Project 6 Earth system models. Models show that after the CO2 concentration and air temperature peaks, land and ocean are decreasing carbon sinks from the 2040s and become sources for a limited time in the 22nd century. The decrease in the carbon uptake precedes the CO2 concentration peak. The early peak of ocean uptake stems from its dependency on the atmospheric CO2 growth rate. The early peak of the land uptake occurs due to a larger increase in ecosystem respiration than the increase in gross primary production, as well as due to a concomitant increase in land-use change emissions primarily attributed to the wide implementation of biofuel croplands. The carbon cycle feedback parameters amplify after the CO2 concentration and temperature peaks due to inertia of the Earth system so that land and ocean absorb more carbon per unit change in the atmospheric CO2 change (stronger negative feedback) and lose more carbon per unit temperature change (stronger positive feedback) compared to if the feedbacks stayed unchanged. The increased negative CO2 feedback outperforms the increased positive climate feedback. This feature should be investigated under other scenarios.

Carbon cycle response to temperature overshoot beyond 2 °C – an analysis of CMIP6 models

I. Melnikova[1,2], O. Boucher[1], P. Cadule[1], P. Ciais[3], T. Gasser[4], Y. Quilcaille[4], H. Shiogama[2], K. Tachiiri[2,5], T. Yokohata[2] and K. Tanaka[2,3]

[1] Institut Pierre-Simon Laplace, Sorbonne Université / CNRS, France

[2] Center for Global Environmental Research (CGER), National Institute for Environmental Studies (NIES), Japan

[3] Laboratoire des Sciences du Climat et de l'Environnement (LSCE), Commissariat à l'énergie atomique et aux énergies alternatives (CEA CNRS UVSQ), Gif-sur-Yvette, France

[4] International Institute for Applied Systems Analysis (IIASA), Austria

[5] Research Institute for Global Change, Japan Agency for Marine-Earth Science and Technology, Japan

[*]Corresponding author: Irina Melnikova (irina.melnikova@ipsl.fr)

Key Points:

- After a peak of CO_2 growth rate in the SSP5-3.4-OS scenario, land and ocean take up carbon for at least 50 years but at a decreasing rate
- The land sink decrease is due to the larger growth of respiration than photosynthetic production and concurrent land-use change emissions
- Under declining emissions, both land and ocean continue to take up carbon at an asymmetrically larger rate

Abstract

There is a substantial gap between the current emissions of greenhouse gases and levels required for achieving the 2 and 1.5 °C temperature targets of the Paris Agreement. Understanding the implications of a temperature overshoot is thus an increasingly relevant research topic. Here we explore the carbon cycle feedbacks over land and ocean in the SSP5-3.4-OS overshoot scenario by using an ensemble of Coupled Model Intercomparison Project 6 Earth system models. Models show that after the CO_2 concentration and air temperature peaks, land and ocean are decreasing carbon sinks from the 2040s and become sources for a limited time in the 22nd century. The decrease in the carbon uptake precedes the CO_2 concentration peak. The early peak of ocean uptake stems from its dependency on the atmospheric CO_2 growth rate. The early peak of the land uptake occurs due to a larger increase in ecosystem respiration than the increase in gross primary production, as well as due to a concomitant increase in land-use change emissions primarily attributed to the wide implementation of biofuel croplands. The carbon cycle feedback parameters amplify after the CO_2 concentration and temperature peaks due to inertia of the Earth system so that land and ocean absorb more carbon per unit change in the atmospheric CO_2 change (stronger negative feedback) and lose more carbon per unit temperature change (stronger positive feedback) compared to if the feedbacks stayed unchanged. The increased negative CO_2 feedback outperforms the increased positive climate feedback. This feature should be investigated under other scenarios.

Plain Language Summary

A large gap between required and currently planned greenhouse gas emission reductions makes possible overshooting the 2 °C target of the Paris Agreement before the temperature can return below the target levels. We explore the response of the global carbon cycle to overshoot by analyzing the simulations of state-of-art models under an overshoot pathway, where the emissions increase until the 2030s and exhibit a steep reduction thereafter. The land and ocean continue to take up carbon from the atmosphere throughout the 21st century, albeit at a reduced rate. The decrease in the ocean carbon uptake occurs before the CO_2 concentration peak due to its dependence on the rate of the atmospheric CO_2 change, and the decrease in the land uptake occurs due to a stronger increase in the ecosystem respiration than in the photosynthetic carbon absorption and simultaneous large land-use-change emissions from the expansion of biofuel crops. After the peaks, land and ocean absorb more carbon from the atmosphere due to higher CO_2 concentration and lose more carbon due to warmer temperatures. The influence of higher CO_2 concentration wins over the influence of warming, allowing land and ocean to remain carbon sinks till the end of the 21st century.

1 Introduction

The Paris Agreement aims for a long-term temperature target of holding global temperature increase well below 2 °C and pursuing efforts to keep warming to no more than 1.5 °C (UNFCCC, 2015). However, there is a substantial gap between the required mitigation efforts to achieve this ambitious target and planned national policies towards emissions reductions. According to the Intergovernmental Panel on Climate Change (IPCC) Special Report "Global warming of 1.5 °C", achieving the temperature target without an overshoot, i.e., temporarily exceeding the 1.5 or 2 °C limits, requires a rapid decline in global net anthropogenic CO_2 emissions by 2030 up to at least 45% for the 1.5 °C and up to at least 25% for the 2.0 °C targets. On the one hand, more than 100 countries have adopted or planned to adopt net-zero targets by the year 2050, and China, which is currently the largest emitter of greenhouse gases (GHGs), promised to become carbon neutral before 2060 (Mallapaty, 2020). On the other hand, current nationally determined contributions indicate a slight increase in the CO_2 emissions in 2030 compared to 2020 levels meaning that current emission pledges may not be enough to achieve the Paris Agreement temperature targets (Höhne et al., 2020). Based on the assessment of current policies, Hausfather & Peters (2020) showed that global warming is on course to exceed 3 °C by the end of this century. Consequently, the possibility of temperature overshoot should be considered by the scientific community.

Our current understanding of the consequences of a temperature overshoot on the carbon cycle is limited. Several studies analyzed the carbon cycle feedbacks in the land and ocean under overshoot scenarios (Boucher et al., 2012; Jones et al., 2016a; Zickfeld et al., 2016; Palter et al., 2018; Schwinger & Tjiputra, 2018; Tokarska et al., 2019; Jeltsch-Thömmes et al., 2020). Using idealized ramp-up and ramp-down scenarios (with increasing and later decreasing CO_2 concentration at a 1% $year^{-1}$ rate). Boucher et al. (2012) and Zickfield et al. (2016) showed that land continues to act as a carbon sink for a long time after the temperature overshoots, while the ocean turns into a source only a few decades after the ramp-down starts. Palter et al. (2018) considered an overshoot scenario, where CO_2 concentration increases until 2060, following a Representative Concentration Pathway (RCP8.5), and rapidly decreases after. They showed that both land and ocean become a carbon source nearly two to three decades after the peaks of CO_2 concentration and temperature. Schwinger & Tjiputra (2018) found that the ocean turns into a carbon source only after a strong reduction in atmospheric CO_2 because the disequilibrium in the sea-air partial pressure is maintained for a long time after the peak of CO_2 concentration. The bottom line is that existing studies all agree that land and ocean act as decreasing sinks at least for a couple of decades after the ramp-down starts, but it is difficult to assess the robustness of the other findings of these studies. Indeed, the studies are based on different, highly idealized scenarios. They also consider a limited number of models, and some of these models are of intermediate complexity with little traceability to more complex models in the context of overshoot scenarios. Thus, the role of more complex processes controlling the response of the carbon cycle to the overshoot of the Paris Agreement temperature target remains largely unexplored.

The response of the carbon cycle to the changes in the atmospheric CO_2 concentrations and climate can be characterized by the carbon cycle feedback framework via carbon-concentration (β) and carbon-climate (γ) feedback parameters, respectively (Friedlingstein et al., 2006; Gregory et al., 2009; Jones et al., 2016b; Schwinger & Tjiputra, 2018; Williams et al., 2019; Arora et al., 2020; Jones & Friedlingstein, 2020). An application of these carbon cycle feedback metrics to an overshoot scenario enables quantification of the contribution of carbon-concentration and carbon-climate feedback to the changes in carbon fluxes before and after the peaks of CO_2 concentration and temperature. The framework has not been used for overshoot scenarios with the exception of Schwinger & Tjiputra (2018) for the ocean. It is important to understand the carbon-concentration and carbon-climate feedbacks of both land and ocean under overshoot scenarios through this feedback framework. The potential reversibility of feedbacks may influence mitigation pathways to achieve the Paris Agreement goals.

In this study, we take advantage of the newly available results from the state-of-art Earth system models (ESMs) developed under the Coupled Model Intercomparison Project 6, CMIP6 (Eyring et al., 2016) simulated under the shared socioeconomic pathway overshooting scenario named SSP5-3.4-OS (O’Neill et al., 2014). First, we evaluate carbon fluxes by ESMs against observational data sets. This step is required because inaccuracies in estimating past carbon uptakes by land and ocean may propagate to future predictions. Next, we investigate the spatiotemporal changes in carbon fluxes by six CMIP6 ESMs. Because the SSP5-3.4-OS includes the implementation of bioenergy crops in the future, we attempt to separate the net land flux into land-use emissions from the expansion of bioenergy crops and sinks or sources in other ecosystems. Finally, we apply the carbon cycle feedback framework to quantify the carbon cycle feedbacks of the CMIP6 ESMs under the SSP5-3.4-OS pathway.

2 Description of the overshoot scenario and Earth system models

2.1 SSP5-3.4-OS

The SSP5-3.4-OS experiment is part of the Scenario Model Intercomparison Project, ScenarioMIP (O'Neill et al., 2017; Tebaldi et al., 2020). It is designed to explore the biogeophysical feedbacks of the Earth system to a strong ramp-down phase of CO_2 concentration and temperature after the historical and future steady increase until the mid-century (Meinshausen et al., 2020). The GHG forcing of the SSP5-3.4-OS is based on the implementation of SSP5 in the REMIND-MAgPIE model and its climate specifications are based on emission-driven runs with MAGICC7.0. The SSP5-3.4-OS initially follows the high emission (fossil-fuel development) SSP5-8.5 scenario and branches from it in 2040. Aggressive mitigation thereafter causes a steep reduction in CO_2 emissions that become net zero by the 2080s, then go net negative up to about -3.8 GtC year^{-1} by the year 2100, and ramp down to zero by the year 2170 (Figure S1). The total radiative forcing in SSP5-3.4-OS reaches 3.4 Wm^{-2} in 2100. The carbon capture and storage (CCS) in this overshoot pathway reaches a cumulative amount of almost 300 GtC (starting from the year 2011) by the end of the 21st century (Figure S1) and is dominated by a second-generation bioenergy cropland expansion, mainly at the cost of pastures (Hurtt et al., 2020).

For the analysis, we use three adjoined experiments— historical from 1850 to 2014, SSP5-8.5 for the period of 2015–2039, and SSP5-3.4-OS for the period of 2040–2100 (2300). In addition to fully coupled simulations (COU), we use biogeochemically (BGC) coupled simulations to study the carbon cycle feedbacks. The SSP5-3.4-OS-BGC is part of the Coupled Climate–Carbon Cycle Model Intercomparison Project, C4MIP (Jones et al., 2016b). As the CO_2 atmospheric concentration is not always reported in the model output, we use directly the input4MIP data set which includes the atmospheric CO_2 concentration pathway used in the concentration-driven simulations (Meinshausen et al., 2016; 2020).

2.2 Earth system models

To date, six CMIP6 ESMs have provided carbon cycle outputs for the SSP5-3.4-OS pathway (Table 1). The models are described in detail elsewhere (Arora et al., 2020; Séférian et al., 2020). Four ESMs (apart from MIROC-ES2L and CESM2-WACCM) provide extended outputs up to the end of the 23rd century. Five ESMs (apart from CESM2-WACCM) provide outputs for both COU and BGC simulations till the end of the 21st century, and the IPSL-CM6A-LR – till the 23rd century. The presence of both COU and BGC simulation outputs enables investigating the carbon cycle feedbacks parameters under the SSP5-3.4-OS scenario. The six models differ in terms of the structure and the representation of carbon cycle processes. Among them, three models represent explicitly the nitrogen cycle over land, two include a fire component, one has dynamic vegetation, and one accounts for permafrost (Table 1). All models simulate inorganic carbon in the ocean, and among them, two models also consider dissolved organic carbon.

For the estimates of the land-use change (LUC) emissions, we use a variable *fLUC* that is present in four models (absent in CanESM5 and MIROC-ES2L). For the analysis, we use the carbon fluxes anomalies relative to the branching year values for changes in carbon pools and long-term mean preindustrial control (piControl) values for changes in carbon fluxes. For both pools and fluxes, we subtract the long-term piControl linear trend to remove any residual trend (Figure S2). In the case of fluxes, we subtract long-term piControl mean values and not the values of branching years to avoid creating a drift caused by the interannual variability. Only one ensemble member was available for all the experiments required. Therefore, for the analysis, we use only one ensemble member of each model documented in Table S1.

Table 1. Major characteristics of the Earth system models, and their simulation setup considered in our study

ESM	IPSL-CM6A-LR	CNRM-ESM2-1	CanESM5	UKESM1-0-LL	MIROC-ES2L	CESM2-WACCM
Center (country)	IPSL (France)	CNRM-CERFACS (France)	CCCma (Canada)	MOHC (UK)	JAMSTEC/NIES/AORI (Japan)	NCAR (USA)
Reference	(Boucher et al., 2020)	(Séférian et al., 2019)	(Swart et al., 2019a)	(Sellar et al., 2019)	(Hajima et al., 2020)	(Danabasoglu et al., 2020)
SSP5-3.4-OS period	2040-2300	2015-2100	2040-2300	2040-2100	2015-2100	2040-2299
Land carbon	ORCHIDEE, br.2.0	ISBA-CTRIP	CLASS-CTEM	JULES-ES-1.0	VISIT-e	CLM5
Nitrogen cycle	No	Implicit	No	Yes	Yes	Yes
Permafrost	No	No	No	No	No	Yes
Fires	No	Yes (natural)	No	No	No	Yes
Dynamic vegetation	No	No	dynamic wetlands	Yes	No	No
PFT	15	16	4 (CLASS), 9 (STEM)	9 natural and 4 crop/pasture	13	22
LUC	Yes	Yes	Yes	Yes	Yes	Yes
Ocean carbon	PISCES-v2	PISCESv2-gas	CMOC	MEDUSA-2.1	OECO2	MARBL-BEC
Representation of marine sediments*	Meta-model	Meta-model	No	Sediment Box	Meta-model	No
SSP-5-3.4-OS-BGC	Yes (extended till 2300)	Yes	Yes	Yes	Yes	No
esm-SSP5-3.4-OS**	No	No	No	Yes	Yes	No
Data set DOIs***	https://doi.org/10.22033/ESGF/CMIP6.5251 https://doi.org/10.22033/ESGF/CMIP6.5195	https://doi.org/10.22033/ESGF/CMIP6.4165 https://doi.org/10.22033/ESGF/CMIP6.4068	https://doi.org/10.22033/ESGF/CMIP6.3673 https://doi.org/10.22033/ESGF/CMIP6.3610	https://doi.org/10.22033/ESGF/CMIP6.6298 https://doi.org/10.22033/ESGF/CMIP6.6113	https://doi.org/10.22033/ESGF/CMIP6.5710 https://doi.org/10.22033/ESGF/CMIP6.5602	https://doi.org/10.22033/ESGF/CMIP6.10094 https://doi.org/10.22033/ESGF/CMIP6.10071

	https://doi.org/10.22033/ESGF/CMIP6.5271 https://doi.org/10.22033/ESGF/CMIP6.5269	https://doi.org/10.22033/ESGF/CMIP6.4221 https://doi.org/10.22033/ESGF/CMIP6.4047 https://doi.org/10.22033/ESGF/CMIP6.4223	https://doi.org/10.22033/ESGF/CMIP6.3696 https://doi.org/10.22033/ESGF/CMIP6.3694 https://doi.org/10.22033/ESGF/CMIP6.3600 https://doi.org/10.22033/ESGF/CMIP6.3697 https://doi.org/10.22033/ESGF/CMIP6.3695	https://doi.org/10.22033/ESGF/CMIP6.6405 https://doi.org/10.22033/ESGF/CMIP6.6397 https://doi.org/10.22033/ESGF/CMIP6.6055 https://doi.org/10.22033/ESGF/CMIP6.6409 https://doi.org/10.22033/ESGF/CMIP6.6401 https://doi.org/10.22033/ESGF/CMIP6.5953 https://doi.org/10.22033/ESGF/CMIP6.5929 https://doi.org/10.22033/ESGF/CMIP6.5969 https://doi.org/10.22033/ESGF/CMIP6.12203	https://doi.org/10.22033/ESGF/CMIP6.5767 https://doi.org/10.22033/ESGF/CMIP6.5582 https://doi.org/10.22033/ESGF/CMIP6.5769 https://doi.org/10.22033/ESGF/CMIP6.5512 https://doi.org/10.22033/ESGF/CMIP6.5496 https://doi.org/10.22033/ESGF/CMIP6.5525	https://doi.org/10.22033/ESGF/CMIP6.10115 https://doi.org/10.22033/ESGF/CMIP6.10114

* from Séférian et al. (2020)

** esm-SSP5-3.4-OS refers to emission-driven simulation, as opposed to concentration-driven SSP5-3.4-OS and SSP-5-3.4-OS – BGC simulations.

3 Evaluation of Earth system models

The historical carbon uptake by land and ocean is relatively well constrained, and the land uptake should be nearly zero when cumulated over the last 200 years (Gruber et al., 2019; Khatiwala et al., 2009). Thus, ESMs that simulate too large a land uptake in the historical period should be treated carefully for future predictions. In this section, we evaluate the ensemble of ESMs that we use in a consistent way against corresponding observational data for understanding inter-model discrepancies.

3.1 Data and methods

We evaluate the land and ocean carbon fluxes using three different approaches. First, we compare the decadal means, interannual variability (IAV), and linear trends in global land and ocean anthropogenic carbon uptakes by ESMs with Global Carbon Budget 2019, GCB2019 v.1.0 (Friedlingstein et al., 2019) in 1985–2018. Here we adopt the GCB2019 net land flux computed as a residual between fossil fuel emissions, atmospheric growth, and the ocean uptake rather than the more uncertain land uptake directly estimated by biogeochemical process models. For evaluation of the ocean uptake, we use both values averaged from models and data-driven products.

Second, we evaluate carbon fluxes in nine regions, covering nearly the entire globe, in six ESMs against the estimates, based on the observations of the REgional Carbon Cycle Assessment and Processes (RECCAP) project further harmonized and completed by additional data and synthesized for 9 land regions covering nearly the entire globe (Ciais et al., 2020), the most comprehensive global bottom-up carbon flux synthesis to date.

The land carbon uptake estimated by Ciais et al. (2020) includes both anthropogenic and natural sinks, unlike GCB2019 that includes only the anthropogenic uptake. For evaluation against both approaches, the NBP anomalies from piControl are used. This causes some level of uncertainty in comparing the land carbon uptake in the nine RECCAP regions and requires careful interpretation.

Finally, the two inversion-based data sets, CarbonTracker 2019 (CT2019) by Jacobson et al. (2020) and Copernicus Atmospheric Monitoring Service (CAMS) by Chevallier (2013) are used to evaluate the spatial variation of the land and ocean carbon uptake in 2000–2014.

3.2 Results of the evaluation

Figure 1 shows the evaluation results of the land and ocean carbon fluxes by ESMs against existing data sets. Note that the observational products of the ocean were corrected to deduce the anthropogenic ocean CO_2 uptake, by removing from their total CO_2 flux estimate a pre-industrial steady-state natural ocean CO_2 outgassing (of about 0.78 GtC year^{-1} from GCB2019). This allows a comparison with the ESMs estimates of anthropogenic ocean uptake relative to their respective piControl (Friedlingstein et al., 2019). The ESMs we considered estimate a higher decadal mean of net land carbon uptake than GCB2019 and slightly underestimate the global mean and IAV of ocean carbon uptake relative to data-driven products (Figure 1a). Among six ESMs, CNRM-ESM2-1 estimates the highest cumulative land carbon uptake and the least cumulative ocean carbon uptake for the 1850-2014 period (Figure S3).

The ESMs agree with the inversions on the ocean acting as a carbon sink globally. Discrepancies are in the tropical areas of the eastern equatorial Pacific Ocean, the northern Indian Ocean, and along the Californian Current. CNRM-ESM2-1 estimates a lower carbon uptake in the North Atlantic Ocean, and MIROC-ES2L estimates weaker outgassing in the equatorial Pacific Ocean than inversions (Figure 1b). These discrepancies were reported by earlier publications (Hajima et al., 2020; Séférian et al., 2019).

The inter-model spread for the net land carbon uptake is much larger than for the ocean sink. GCB2019 reports a smaller net land carbon sink (including LUC emissions) on average during 1985–2018 than ESMs (Figure 1a). The higher land sink by CNRM-ESM2-1 and MIROC-ES2L in the historical period than GCB2019 and other ESMs corresponds to a larger increase in the land carbon pools (Figure S3). IPSL-CM6A-LR is the closest to GCB2019 in terms of the IAV of the land sink (defined via standard deviation) among the ESMs. MIROC-ES2L and UKESM1-0-LL estimate higher IAV, and CNRM-ESM2-1 and CESM2-WACCM underestimate lower IAV than GCB2019. The spatial variations of the net land carbon uptake by the two atmospheric inversions agree in sign but disagree in magnitude with each other, even at the scale of coarse latitude bands (Friedlingstein et al., 2019 and Figure 1b). The inversions estimate a higher land sink in the north than ESMs and a carbon source in the tropics that is not present in the ESMs. MIROC-ES2L estimates a slightly higher net biome production (NBP) sink in Northern Hemisphere than other models (that is still lower than in the inversions). UKESM1-0-LL estimates slightly high carbon uptake in tropical Amazonia and Africa, which Sellar et al. (2019) attributed to a small overestimation of tree fraction in savanna biomes compared to observational data sets.

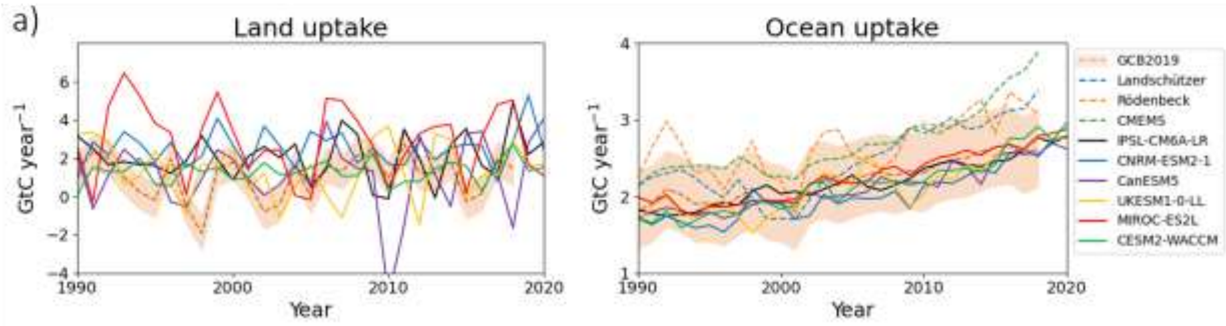

	Land (1985-2018)							Ocean (1985-2018)									
	GCB2019 (Residual)	IPSL-CM6A-LR	CNRM-ESM2-1	CanESM5	UKESM1-0-LL	MIROC-ES2L	CESM2-WACCM	GCB2019	IPSL-CM6A-LR	CNRM-ESM2-1	CanESM5	UKESM1-0-LL	MIROC-ES2L	CESM2-WACCM	Landschützer	Rödenbeck	CMEMS
Mean	**0.04**	1.81	2.36	1.05	1.30	2.99	1.20	**2.14**	2.08	1.91	2.02	2.05	2.16	2.04	1.63	1.85	1.80
IAV	**1.21**	1.29	0.76	1.77	1.49	1.82	0.65	**0.30**	0.31	0.33	0.28	0.34	0.31	0.35	0.45	0.36	0.50
Slope	**0.04**	0.04	0.00	-0.02	0.00	0.00	0.02	**0.03**	0.03	0.03	0.03	0.03	0.03	0.03	0.04	0.02	0.05

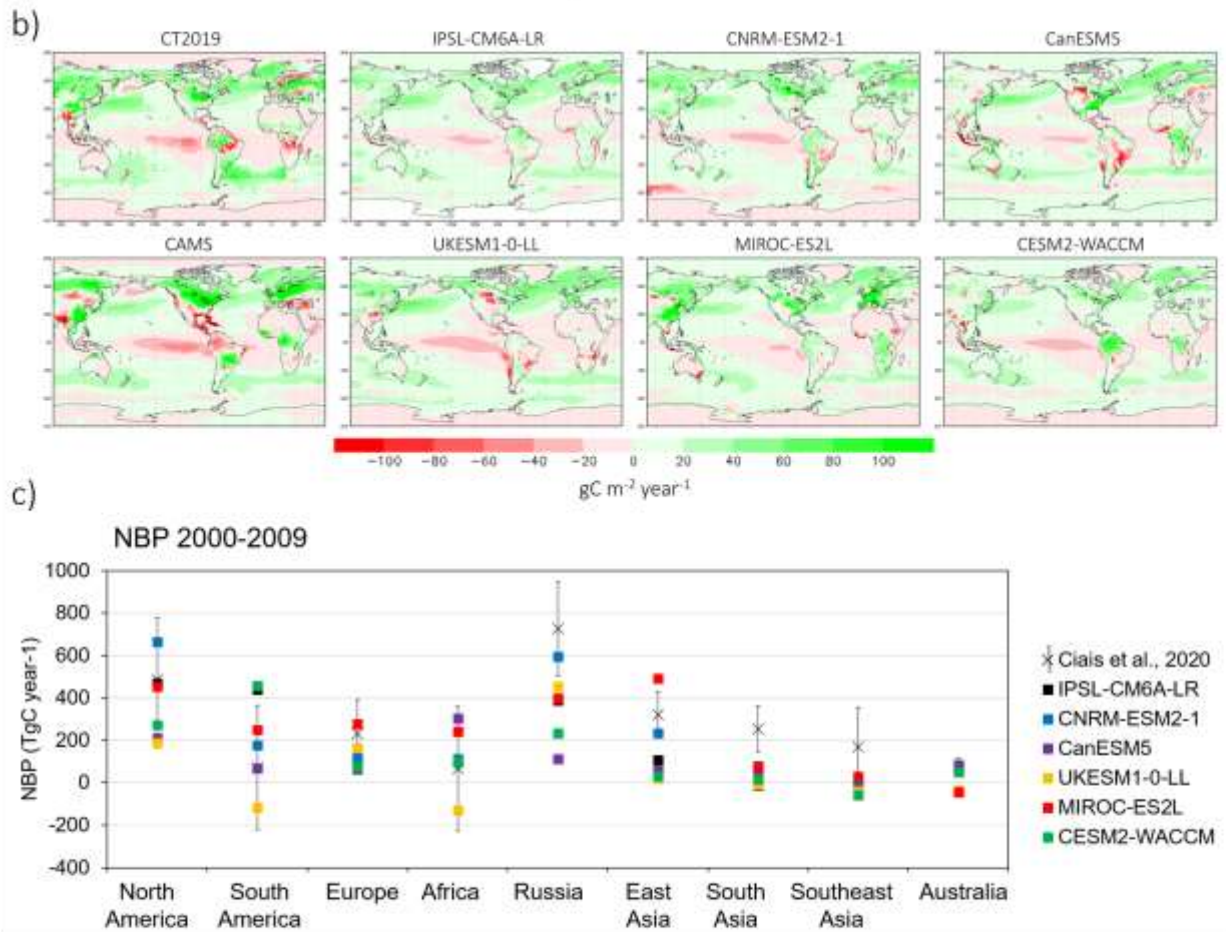

Figure 1. An evaluation of Earth system models (ESMs) against observational and inversion datasets. The sign convention is that sources of CO_2 to the atmosphere are negative values and removals/sinks are positive. Panel (a) shows the interannual variability of land (net biome

production, NBP) and ocean (fgco2) carbon uptakes by ESMs and Global Carbon Budget (GCB2019) and three data-driven products (Denvil-Sommer et al., 2019; Landschützer et al., 2016; Rödenbeck et al., 2014). Data-driven products are corrected for pre-industrial outgassing of 0.78 GtC year^{-1}. Shaded area indicates uncertainty provided by Friedlingstein et al. (2019). The residual NBP values for GCB2019 in the table are calculated using the GCB2019 ocean uptake that is the average of several global ocean biogeochemistry models that reproduce the observed mean ocean sink of the 1990s and are compared to the NBP anomaly from piControl by ESMs. Panel (b) shows the 2000–2014 mean annual carbon uptake by land and ocean estimated by ESMs and two atmospheric inversions CT2019 and CAMS. Panel (c) shows NBP for nine RECCAP regions in 2000–2009 according to Ciais et al. (2020). Error bars indicate estimates of uncertainty from Ciais et al. (2020).

All ESMs estimate lower land carbon uptake in Russia, South Asia, and Southeast Asia than the corresponding inventory-based estimates in RECCAP (Figure 1c). To understand the reasons for this underestimation, we compared other land fluxes by ESMs with those given by Ciais et al. (2020) (Figure S4). ESMs adequately estimate net primary production (NPP) relative to RECCAP. CESM2-WACCM and IPSL-CM6A-LR reproduce heterotrophic respiration (R_H) well. However, most models estimate higher than RECCAP estimates R_H in North America, East Asia, South-East Asia, and Australia, possibly because they do not include harvest processes that decouple NPP from R_H. The *fLUC* emissions are underestimated by ESMs in tropical regions. This likely reflects the fact that *fLUC* diagnosed by ESMs follows a definition that does not cover all LUC emission terms of the models' realm (e.g., legacy soil carbon emissions after LUC, biomass decay after LUC are not in *fLUC*). There is also the fact that models do not reproduce some LUC emission processes such as shifting cultivation or degradation that were included in the LUC emissions from RECCAP. The difference between NPP and R_H is higher in RECCAP estimates than in ESMs in all regions. Thus, these component fluxes cannot explain the discrepancies between ESM and RECCAP estimates, suggesting there could still be missing processes in these state-of-the-art models (Ciais et al., 2020).

The CMIP6 ESMs show higher historical land carbon uptake than GCB2019 and lower uptake than estimates by Ciais et al. (2020). This is probably due to the differences in terms included in the land sink by two evaluation approaches – anthropogenic sink in GCB2019 and anthropogenic and natural sinks in the study by Ciais et al. (2020). However, the use of both NBP anomaly from piControl (Figure 3c) and NBP absolute value (Figure S4d) lead to very similar results. Whether the natural or anthropogenic terms of land uptake in certain regions were underestimated requires further analysis and more attention in future studies.

4 Analysis of the carbon cycle feedbacks under the SSP5-3.4-OS pathway

4.1 Temporal variation of global carbon fluxes under SSP5-3.4-OS

In the concentration-driven SSP5-3.4-OS scenario, the CO_2 concentration as given by input4MIPs peaks in the year 2062 at 576.2 ppm (Figure 2). According to the scenario design, strong mitigation policies to reduce GHGs emissions, which include bioenergy crops and CCS (BECCS), start in 2040 and result in an immediate decrease in the CO_2 growth rate that peaks in 2041 (O'Neill et al., 2017; Meinshausen et al., 2020). Both peaks of the CO_2 concentration and CO_2 growth rate have important implications on the carbon fluxes discussed hereafter.

The six ESMs demonstrate large differences in the response of global mean surface air temperature (GSAT) to the prescribed changes in CO_2 concentration under the SSP5-3.4-OS. The magnitudes of the overshoot vary from 2.4 °C in MIROC-ES2L to 4.1 °C in CanESM5, the timings of the GSAT peaks vary from the late 2040s in MIROC-ES2L to the late 2070s in CNRM-ESM2-1, and the rates of the GSAT ramp-down vary from a steep decrease in CanESM5 to almost no decrease in CNRM-ESM2-1. The multi-model mean GSAT is 2.32 ± 0.28 °C at the end of the 23rd century. Its temporal trajectory differs among ESMs from a weak persistent decrease in CanESM5 and IPSL-CM6A-LR to an increase in CESM2-WACCM and CNRM-ESM2-1. In all six ESMs, the growth rate of GSAT peaks in the early 2040s, just a few years after the peak of the CO_2 growth rate (Figure S5a).

A previous idealized scenario-based study reported that the transient climate response to cumulative carbon emissions (TCRE) is larger in the ramp-down period than in the ramp-up period of carbon emissions (Zickfeld et al., 2016). Our analysis could not confirm this, as the majority of ESMs showed a decrease in TCRE during the ramp-down period (Figure S5b). The inter-model differences in TCRE may be related to the model parametrization, and particularly the effective equilibrium climate sensitivity (ECS) as pointed out by Tachiiri (2020). However, further investigation is necessary for a deeper understanding of the underlying reasons for the inconsistency between 1%-increase idealized and more societally relevant SSP5-3.4-OS.

The land and ocean carbon uptakes always decrease after the peak of the CO_2 growth rate (and before the peak of CO_2 concentration). However, these two reservoirs continue to remove CO_2 from the atmosphere at least for 50 years (Figures 2b and 2c). ESMs with COU simulation extended outputs till the 22nd and 23rd centuries show that the land and ocean turn into a carbon source for a limited time in the 22nd century. At the end of the 22nd century, the land becomes nearly net-zero and the ocean remains a weak carbon sink. Among ESMs, CESM2-WACCM –that accounts for permafrost processes– has the lowest value of land carbon uptake (zero to weak source) at the end of the 23rd century. It simulates a continued carbon source from high latitude carbon soils till the end of the study period that is almost entirely compensated by the vegetation greening (Figure S6). By the end of the 23rd century, the accumulated carbon is stored mainly in the Southern Ocean and over mid-to-high latitudes of the Northern Hemisphere in the land. When looking at the changes in the carbon reservoirs (Figure S3), the ESMs agree that during the ramp-down, the ocean releases some previously-stored carbon to the atmosphere for a limited period (of around 50 years) and continues to take up carbon at a decreased rate thereafter. The long-term response of land to the overshoot largely differs among ESMs to the extent from returning to the preindustrial levels of carbon storage in CanESM5 to the increase in land carbon pool half the size of the cumulative ocean flux in IPSL-CM6A-LR and twice the size of the cumulative ocean flux in CNRM-ESM2-1.

The estimated behavior of land and ocean under overshoot is consistent with existing studies. Jones et al. (2016a) used four ESMs and RCP2.6 scenario, which has an earlier peak of CO_2 growth rate (and CO_2 concentration) and a slower ramp-down phase than this study. They reported that land and ocean remain carbon sinks for more than 100 years after the peak of the CO_2 growth rate. Palter et al. (2018) used one ESM and RCP8.5-based overshoot scenario, which has a later peak of CO_2 growth rate (and CO_2 concentration) and a more rapid ramp-down phase than this study. They reported that land and ocean turn to carbon sources in less than three decades after the peak of CO_2 concentration. Based on the three studies, earlier CO_2 peak and slower ramp-down cause the land and ocean to act as carbon sinks for a longer time.

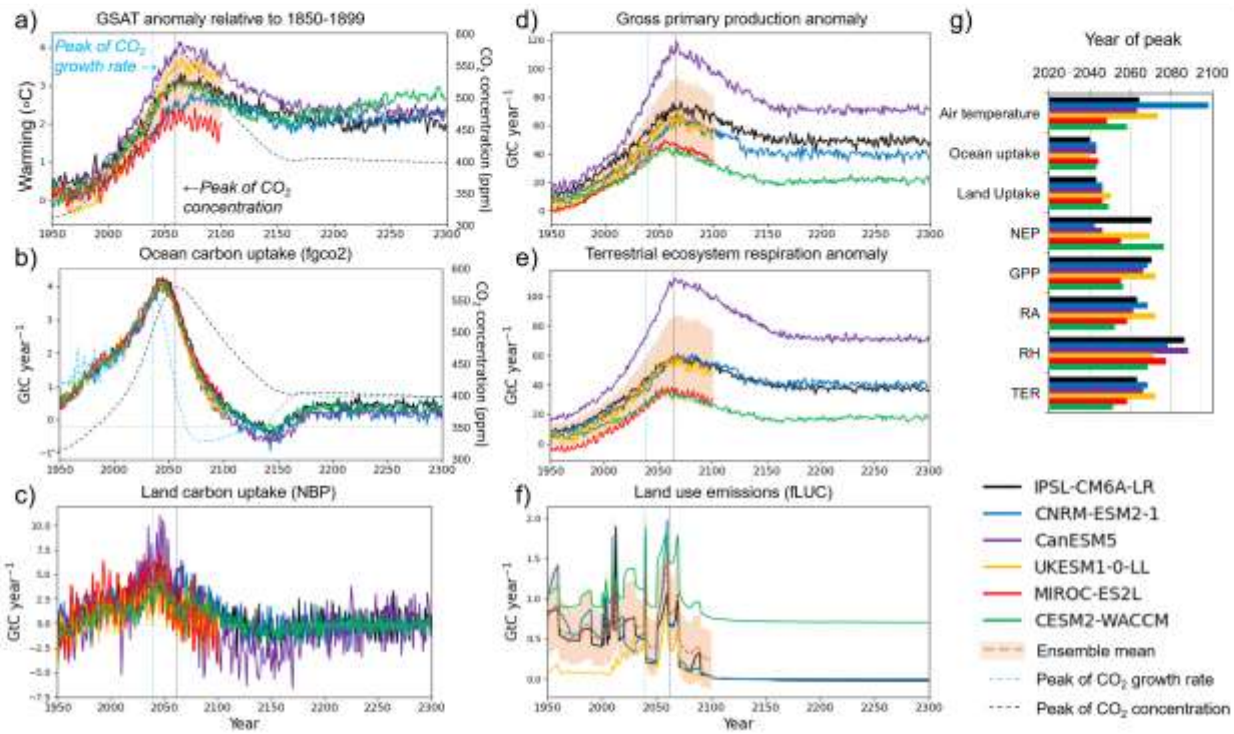

Figure 2. Time series and peak years of the global annual total or mean variables of ESMs, including (a) GSAT, and CO_2 concentration, (b) ocean uptake, (c) NBP, (d) GPP, (e) TER, and (f) LUC emissions. Air temperature anomaly is taken from 1850–1899 mean; other variables are anomalies from piControl simulation. The ensemble mean (dashed brown line) of six ESMs is calculated till the year 2100 with a shaded area indicating ensemble spread via standard deviation. The CO_2 concentration and its growth rate are shown with dashed black and blue curves on panels (a) and (b). The years of peak atmospheric CO_2 concentration and CO_2 growth

rate are indicated by vertical black and blue dashed lines, respectively. Panel (g) indicates the years of peak of the variables.

4.2 The peaks of land and ocean carbon uptakes

The peaks of carbon uptake by land and ocean occur before the peaks of CO_2 concentration, temperature, gross primary production (GPP), terrestrial ecosystem respiration (TER), and its components autotrophic (R_A) and heterotrophic (R_H) respirations (of which R_H peaks the latest). To identify the reasons for those varying peak times, it is essential to look at the derivatives of the variables (Figures S7).

The response of air temperature lags CO_2 concentration, owing to the inertia of the climate system at the time the CO_2 starts to decrease. McKinley et al. (2020) and Schwinger and Tjiputra (2018) pointed out that the CO_2 growth rate dominates the variability in the global ocean on year-to-year timescales, hypothesizing that other internal and external drivers may become more important in the altered state of the ocean in the future. Using the outputs of six CMIP6 ESMs, we show that global ocean carbon uptake is nearly a linear function of the atmospheric CO_2 growth rate, confirming the finding discussed above. The slope of the function changes after the peak of the CO_2 growth rate from 0.74 ± 0.03 to 0.26 ± 0.02 GtC year^{-2} (average and standard deviation of six ESMs), with a clear hysteresis behavior (Figure 3b). At the peak of the CO_2 growth rate, the linear function curls up with the negative CO_2 growth values. The extended simulation outputs available for four models indicate that the trajectory of the ocean uptake curve is directed towards zero, closing the cycle after a limited period of carbon source.

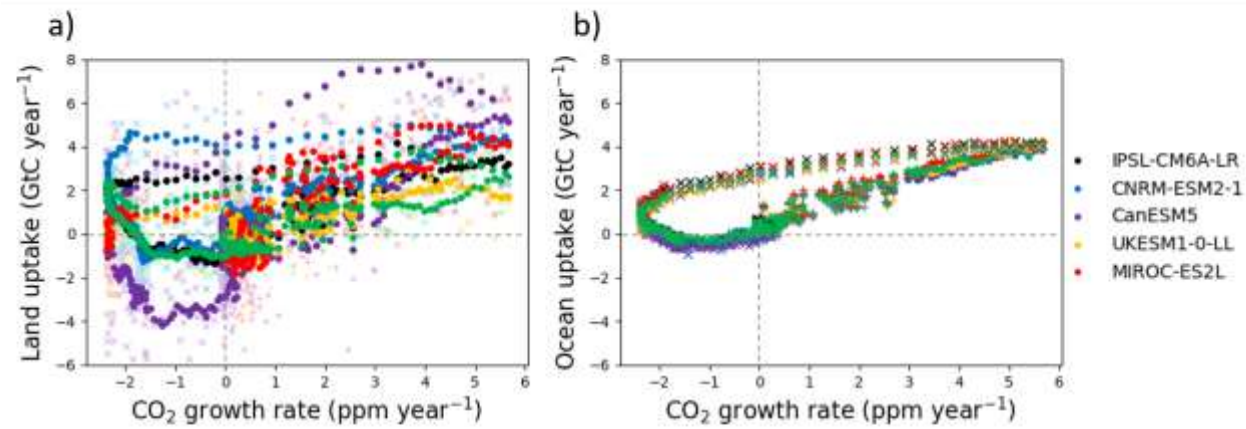

Figure 3. The dependency of (a) land and (b) ocean carbon uptake on the atmospheric CO_2 growth rate by CMIP6 Earth system models under historical and SSP-5-3.4-OS pathway. The markers "+" indicate the historical period (1850–2014), markers "*" and "×" indicate the periods before and after the peak of CO_2 growth rate in 2041, respectively. In the case of the land uptake, the points correspond to decadal moving averages, annual points are shown in pale colors.

The ESMs reveal a weaker linear dependency of the land carbon uptake on the CO_2 growth rate than on the ocean uptake (Figure 3a). It is well-known that the two largest land carbon fluxes, namely GPP and TER, primarily depend on the CO_2 concentration, temperature, and soil moisture, as well as other factors not modeled by ESM such as land management intensity, and nutrient limitations (Ciais et al., 2020; Huntzinger et al., 2017). In addition, land carbon uptake experiences much larger interannual variability. When the interannual variability is removed, the linear dependency of the land uptake on the CO_2 growth rate becomes nearly parallel to that of ocean uptake.

The nearly linear dependency of the land and ocean carbon uptakes on CO_2 growth rate characterizes the system response to the forcing rate of change (CO_2 growth rate), i.e., the level of departure from the existing equilibrium state. The hysteresis behavior during the ramp-down period indicates how the system responds to the forcing magnitude (CO_2 concentration). Figures 2 and 3 suggest that on short time-scales, the changes in the land and ocean carbon uptakes are strongly related to the state disequilibrium. The greater the disequilibrium is, (i.e., the larger the CO_2 growth rate is), the larger the responses of the land and ocean carbon uptakes are. In the longer time scales, e.g., timescales longer than carbon residence time in the pool, the changes in the land and ocean carbon uptakes may be strongly related to the state of the system itself. Previously, Koven et al. (2015) showed an apparent reduction in the soil carbon residence time when the forcing rate is too fast because carbon only goes through the fast pools and returns to the atmosphere. We showed that this may be true for land and ocean carbon pools. Future studies should further investigate this feature.

4.3 Impact of land-use change emissions

The changes in the growth rate of GPP and TER alone cannot explain the early land carbon uptake peak in some models, e.g., IPSL-CM6A-LR. The BECCS-related anthropogenic LUC emissions in the 2040s may also contribute to the early peak of the land carbon uptake although models do not represent explicitly the higher yield or specific biophysical parameters of bioenergy crops (to our knowledge). In the SSP5-3.4-OS, the only type of anthropogenic carbon emissions that increases after the 2040s is that of agriculture, forestry, and other land use (AFOLU, Figure S8). We postulate that both the larger growth rate of TER than GPP and increased LUC emissions cause the early peak of land uptake. The expansion of biofuel crops may cause a weakening of the land sink capacity because these systems dedicated to biomass production for harvest no longer have the potential for storing carbon e.g., in soils or biomass.

The spatiotemporal variation of the bioenergy cropland area under the SSP5-3.4-OS is formulated in the Harmonization of Global Land-Use Change and Management (LUH2) data set (Hurtt et al., 2020). In most ESMs, the areas where the bioenergy crops are implemented correspond to areas of decreases in the land carbon uptake after the CO_2 growth rate peaks compared to the prior period, e.g., eastern South America, Europe, the eastern coast of North America, and the northern part of Southeast Asia (Figures S7b, S9, and S10). A strong impact of LUC on the carbon uptake is remarkable for the IPSL-CM6A-LR and UKESM1-0-LL. Yet, the effect of LUC on newly converted bioenergy croplands vs. those of climate change on remaining natural ecosystems cannot be separated in each ESM grid cell, from the available simulations. The modeling groups use varying definitions of the land-use change due to different system boundaries and different definitions of the human perturbation of ecosystems resulting in inconsistent reporting of LUC emissions estimates among the ESMs (Gasser & Ciais, 2013). This uncertainty should be addressed in related future intercomparison projects.

5 Quantifying the Carbon cycle feedbacks under the SSP5-3.4-OS pathway

5.1 Definitions and method

We apply the carbon cycle feedback framework on the five ESMs (apart from CESM2-WACCM) that have all the necessary data for calculations explained below. The carbon-concentration feedback parameter (β, GtC ppm^{-1}) indicates the changes in the carbon storages of land and ocean in response to changes in the atmospheric CO_2 concentration. The carbon-climate feedback parameter (γ, GtC $°C^{-1}$) indicates the changes in the carbon storage in response to the changes in GSAT. The change in the carbon storages of land and ocean can then be decomposed into the β and γ contributions ($\beta \times \Delta CO_2$ and $\gamma \times \Delta T$, respectively), and a residual term ε:

$$\Delta C = \beta \times \Delta CO_2 + \gamma \times \Delta T + \varepsilon \qquad (1)$$

The β contribution (or β uptake) is the changes in carbon storage (GtC) or flux (GtC year^{-1}) credited to the carbon-concentration feedback and γ contribution is the changes in carbon storage or flux credited to the carbon-climate feedback. ΔC is the difference in the carbon storage relative to the piControl simulation, ΔCO_2 is the difference in the global atmospheric CO_2 concentration relative to the value of the year 1850 as given by input4MIP (284.32 ppm), and ΔT is the difference in temperature simulated by each ESM relative to 1850–1899 mean GSAT. In the case of the SSP5-3.4-OS, neither ΔCO_2 nor ΔT become negative any time after the peaks.

The carbon cycle feedback parameters can be diagnosed from the differences in COU, BGC, and radiatively coupled (RAD) simulations of ESMs. In the BGC simulation, only changes in the CO_2 concentration, and not temperature, affect the land and ocean carbon-cycle processes. In the RAD simulation, in contrast, changes in the CO_2 concentration affect the radiation balance of the atmosphere but are not seen by the carbon cycle. There are two commonly used approaches to estimate the carbon cycle feedback parameters, (1) β from BGC, γ from RAD, and (2) β from BGC, γ from the difference between COU and BGC (thereafter, COU–BGC). In this study, we used the latter approach because no RAD simulations are currently available for SSP5-3.4-OS. In this case, the residual term ε of Equation (1) is integrated into γ. Previous studies show that the absolute values of γ estimated by the COU–BGC approach can appear 2–3 times larger than the RAD approach because RAD simulation does not include the suppression of carbon transport to the deep ocean due to weakening ocean circulation (Schwinger & Tjiputra, 2018; Arora et al., 2020).

We estimate β and γ for land (β_{land} and γ_{land}) and ocean (β_{ocean} and γ_{ocean}) using the land carbon pool (*cLand*) and cumulative ocean carbon flux (*fgco2*) because not all models provide the ocean carbon pools (*dissic* and *dissoc*). Before calculations, we confirmed that β and γ estimated using the carbon pool variables agree with corresponding estimates obtained from the cumulative carbon fluxes, i.e., *NBP* and *cLand* over land and *fgco2* and *dissic+dissoc* over the ocean (not shown). Furthermore, we decomposed the land β in terms of underlying processes, such as GPP, R_A, and R_H, using cumulative fluxes over time.

5.2 Carbon cycle feedbacks before mitigation activities

The β and γ feedback parameters depend on the state of the system and scenario (Friedlingstein et al.; 2006, Jones et al., 2016b; Willeit et al., 2014). To understand the carbon cycle feedbacks under the SSP5-3.4-OS overshoot pathway, it is essential to first investigate the changes in the carbon pools (that define the state of the system) over the historical period. ΔC of the five ESMs varies in the historical period to the extent that ΔC_{land} is either positive, e.g., in CNRM-ESM2-1, IPSL-CM6A-LR, and UKESM1-0-LL, or negative, e.g., in CanESM5 and MIROC-ES2L (Figure S3), resulting in positive and negative β (Figures 4 and 5) at the beginning of the 21st century. The negative β in some models is likely a result of decreases in the carbon storage due to LUC emissions.

Before the peak of CO_2 concentration, β_{ocean} decreases (becomes less positive) in all five ESMs (Figure 4a) because increasing anthropogenic carbon emissions exceed the ability of the ocean to absorb carbon (Friedlingstein et al., 2006; Gregory et al., 2009). In all models apart from CNRM-ESM2-1, β_{land} increases at the beginning of the 21st century and continues to increase after the CO_2 concentration peak at a rising rate. CNRM-ESM2-1 exhibits larger uptake during the historical period before the year 2000 that, perhaps, causes high ΔC already at the beginning of the 21st century, leading to overly high β_{land}. Besides, unlike other models, CNRM-ESM2-1 shows decreasing positive γ_{ocean} throughout the study period.

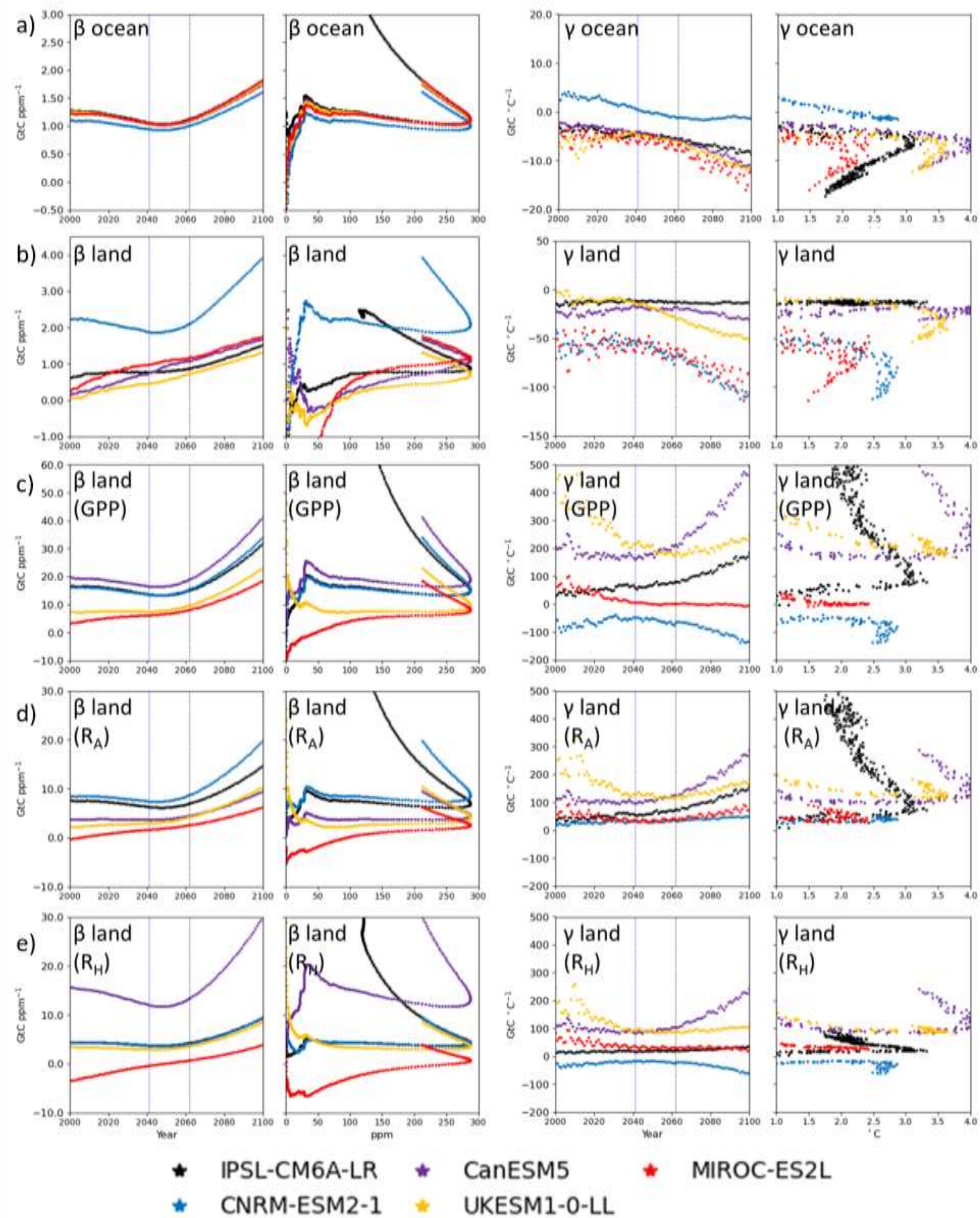

Figure 4. Carbon-concentration β (GtC ppm^{-1}) on the left and carbon-temperature γ (GtC °C^{-1}) feedback parameters for (a) ocean estimated from cumulative flux fgco2, and (b) land estimated

from cumulative NBP. Estimated feedback parameters for cumulative land fluxes: (c) GPP, (d) $R_{A,}$ and (e) R_H. The figures in the first column show β as a function of time (year) and in the second column as a function of ΔCO_2 concentration (ppm). The figures in the third column show γ as a function of time (year) and in the fourth column as a function of temperature (°C). GPP, NBP, and fgco2 are positive to the surface, R_A and R_H are positive to the atmosphere. We use data extended to 2300 for IPSL-CM6A-LR. In the first and third columns, the years of peak atmospheric CO_2 concentration and CO_2 growth rate are indicated by vertical black and blue dashed lines, respectively.

5.3 Magnitudes of carbon cycle feedbacks under SSP5-3.4-OS

Apart from CNRM-ESM2-1, the strength of the β feedback parameter by ESMs is similar over land and ocean, the strength of the negative γ parameter is larger over land than over ocean (Figures 4a and 4b). The magnitude of global transient γ_{land} at the maximum exceeds γ_{ocean} nearly 1.5 times in IPSL-CM6A-LR, 2–3 times in CanESM5 and UKESM1-0-LL, and 10–20 times in CNRM-ESM2-1 and MIROC-ES2L. This agrees with a study based on the idealized 1% CO_2 increase 2 × CO_2 and 4 × CO_2 scenarios (see Table A1 of Arora et al., 2020) and persists in both ramp-up and ramp-down stages of overshoot. The inertia of the Earth system causes an increase in the absolute values of β and γ after the peaks of CO_2 and temperature, i.e., more positive β and more negative γ (Figure 4).

IPSL-CM6A-LR is the only ESM that included both extended to the 23rd century BGC and COU simulations that are necessary for the calculation of β and γ. At the end of the 23rd century, CO_2 concentration is around 398 ppm and air temperature warming relative to pre-industrial value is around 1.9 °C. This ESM, unlike others, estimated nearly constant γ_{land}. The model outputs show a continued amplification of β_{ocean} and γ_{ocean} at a reduced rate after the 2150s and nearly constant β_{land} and γ_{land} after the 2150s (Figure S11). This behavior of β and γ translates into nearly steady states of land and ocean carbon fluxes (Figure 2). By the end of the 23rd century, land and ocean storages increase by 180 and 416 GtC relative to the preindustrial levels, respectively.

The LUC effects on the global carbon cycle feedbacks may be increasingly strong in the future mitigation pathways (see Section 4.3). The amplification of global β_{land} may be reduced due to the conversion of large areas to biofuel croplands. The impacts of LUC on the global γ_{land} are even more uncertain. This uncertainty should be tackled in future studies as well as in a possible future MIP study.

5.4 Decomposition of β_{land} and γ_{land} into the β and γ of their constituent gross fluxes

We decompose β_{land} and γ_{land} into the β and γ of their constituent gross fluxes, to investigate the processes behavior before and after the peaks of CO_2 and temperature (Figures 4, 6, S14 and S15). β of GPP, R_A, and R_H (β_{GPP}, β_{RA}, and β_{RH}) exhibit similar behavior with a nearly parallel change, albeit with an opposite impact on the land uptake (Figures 4 c–e). All ESMs demonstrate a larger β_{GPP} than β_{RA} and β_{RH} together, which provokes positive β_{land} feedback during the study period. Global values of γ_{GPP}, $\gamma_{RA,}$ and γ_{RH} are positive, except for CNRM-ESM2-1, while they are negative in the equatorial region for most ESMs (Figure S16). This means that warmer temperatures under the SSP5-3.4-OS do not inhibit photosynthetic processes in the warm regions to a level that surpasses the benefits of warming on the global ecosystem.

Unfortunately, most ESMs used in this study did not include permafrost or vegetation fire components. By considering permafrost emissions, which roughly speaking are equivalent to γ becoming more negative, Gasser et al. (2018) estimated that to achieve the 2 °C target of the Paris Agreement, the remaining emission budget is reduced by 16% for 0.5 °C overshoot and by 25% for 1 °C overshoot. CESM2-WACCM, the only ESM we considered that resolves the permafrost active layer, did not have BGC simulation outputs under the SSP5-3.4-OS pathway at the time of this analysis. While it would be extremely interesting to look at the carbon cycle feedbacks simulated by this model, its land and ocean carbon uptake estimates nearly median temporal variation of the carbon uptakes among our five ESMs (Figure 2). Based on the spatiotemporal variation of soil carbon storage by the model (Figure S6), we speculate that the permafrost fluxes are not significant in this scenario. Although in CESM2-WACCM, after the air temperature peaks in 2058 (Figure 2), the land pool loses soil carbon in the high latitudes, the loss is mainly attributed to medium soil pool with residence time <100 years (not shown), and it is compensated by vegetation greening in the region. The permafrost fluxes may become significant for larger magnitudes of temperature overshoot, and it is necessary to explore permafrost feedback under different overshoot pathways.

5.5 Spatial variation of transient carbon cycle feedbacks under overshoot

The spatiotemporal variation of the changes in β and γ parameters clarifies the inter-model differences (Figure 5). β_{ocean} strengthens during the ramp-down in the mid-latitudes of the Northern Hemisphere and equatorial zone and increases over the Southern Ocean. In many areas of β_{ocean} increase, γ_{ocean} also intensifies, perhaps, due to the increases in the ocean pool.

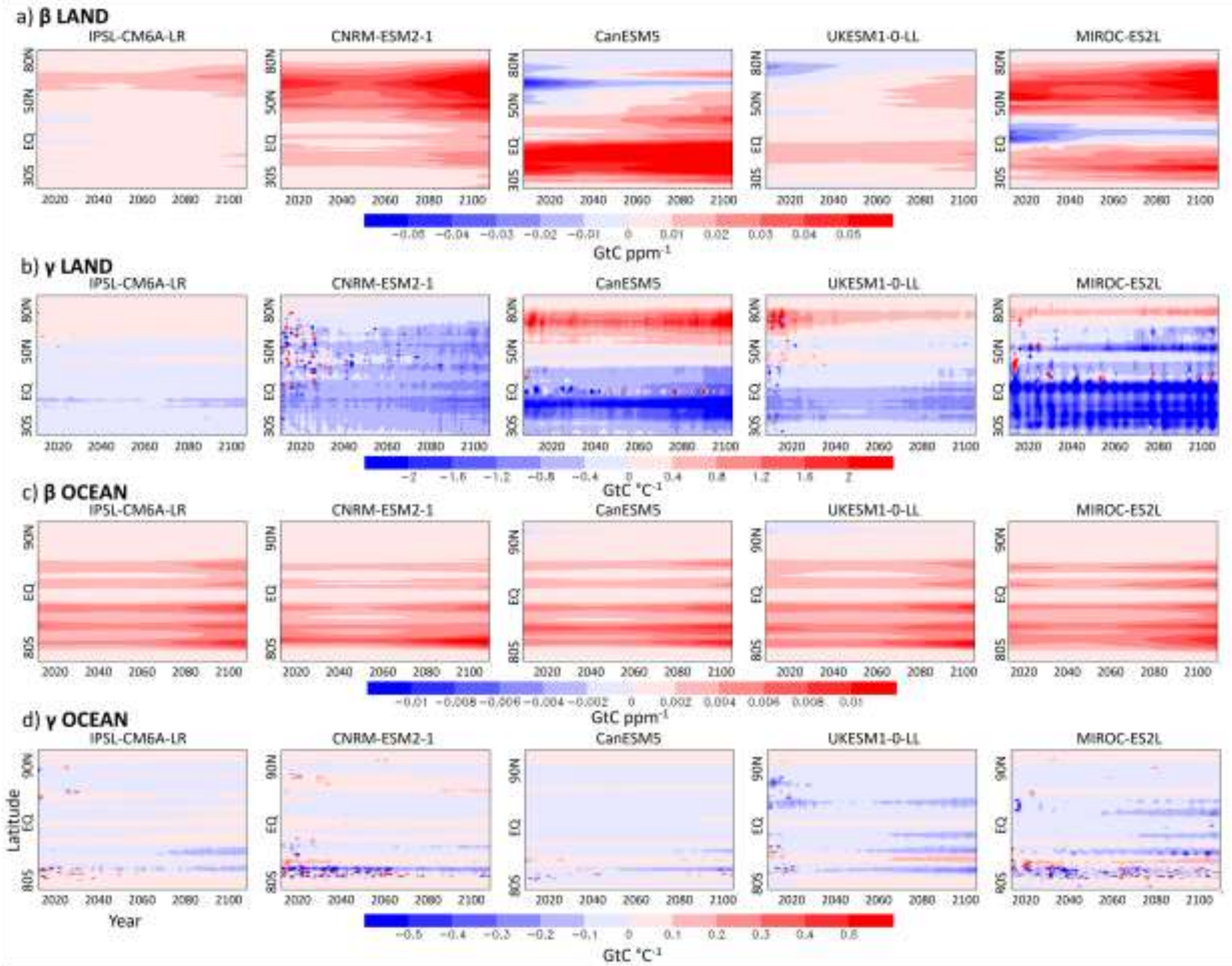

Figure 5. The spatiotemporal variation of zonal cumulative (a) β_{land} (GtC ppm^{-1}), (b) γ_{land} (GtC °C^{-1}), (c) β_{ocean} (GtC ppm^{-1}) and (d) γ_{ocean} (GtC °C^{-1}) calculated from land carbon pool and cumulative ocean uptake. Positive values indicate a net sink.

The spatial variation of β_{land} and γ_{land} is strikingly diverse among models. ESMs agree that β_{land} is positive in the equatorial region, and it increases during the ramp-up but decreases during the ramp-down. CanESM5and UKESM1-0-LL have negative β_{land} over mid-latitudes till the 2040s that is compensated by the positive γ_{land}. The negative γ_{land} over tropics in MIROC-ES2L is maintained throughout the study period, although it keeps decreasing (Figure 5). The negative β_{land} emerges due to the decrease of ΔC_{land} below the pre-industrial value before ramping back by the end of the 21st century (Figures S3 and S12). The decrease in ΔC_{land} corresponds to the decrease in ΔC_{soil} in CanESM5, and ΔC_{veg} in MIROC-ES2L and UKESM1-0-LL.

The γ_{land} is positive in the high latitudes and negative in the equatorial regions, as estimated by all ESMs except for CNRM-ESM2-1. The distinct changes in CNRM-ESM2-1 in the idealized scenarios were discussed by Arora et al. (2020) and attributed to the larger nonlinearity effects compared to other models. The negative γ_{land} in CNRM-ESM2-1 emerges due to negative γ_{soil}, while γ_{veg} stays positive through the study period (Figure S13). After the peak of air temperature, the γ_{land} is increasingly negative in the equatorial zone (probably due to drying, Figure 5b). Overall, our results imply that the amplification of the β_{land} after overshoot is driven by the high latitudes, and the amplification of γ_{land} is driven by the equatorial regions.

5.6 Implication of changes in carbon cycle feedback metrics to the carbon fluxes under overshoot

Due to the dependency of the β uptake on the CO_2 growth, it starts to decrease in the early 2040s, leading to the peaks of the land and ocean uptakes in 2040s concurrent with the peak of CO_2 growth rate (Figures 6a and 6b). The γ uptake peaks later due to temperature change lagging behind the atmospheric CO_2 change. Although the values of β and γ parameters (>0 for β and <0 for γ) increase after the peaks of CO_2 and temperature, opposing each other, the total γ-driven loss of carbon is smaller than β gain at least till the end of the 21st century. The changes in the carbon cycle are dominated by β rather than γ. While existing studies show that during the ramp-up period, the positive contribution of the β is larger than the γ-driven loss (Arora et al., 2020), we demonstrate here for the first time that this remains valid for the ramp-down period under SSP5-3.4-OS based on the five CMIP6 ESMs under consideration.

Apart from CNRM-ESM2-1 that has positive γ_{ocean}, ESMs show that the amplification of β_{ocean} and γ_{ocean} during the ramp-down period cause the ocean to uptake more carbon compared to if β_{ocean} and γ_{ocean} were fixed at the level of the peaks of CO_2 concentration and temperature. All models agree that amplification β_{land} and γ_{land} lead to a larger cumulative land carbon uptake by the year 2100 under the SSP5-3.4-OS pathway.

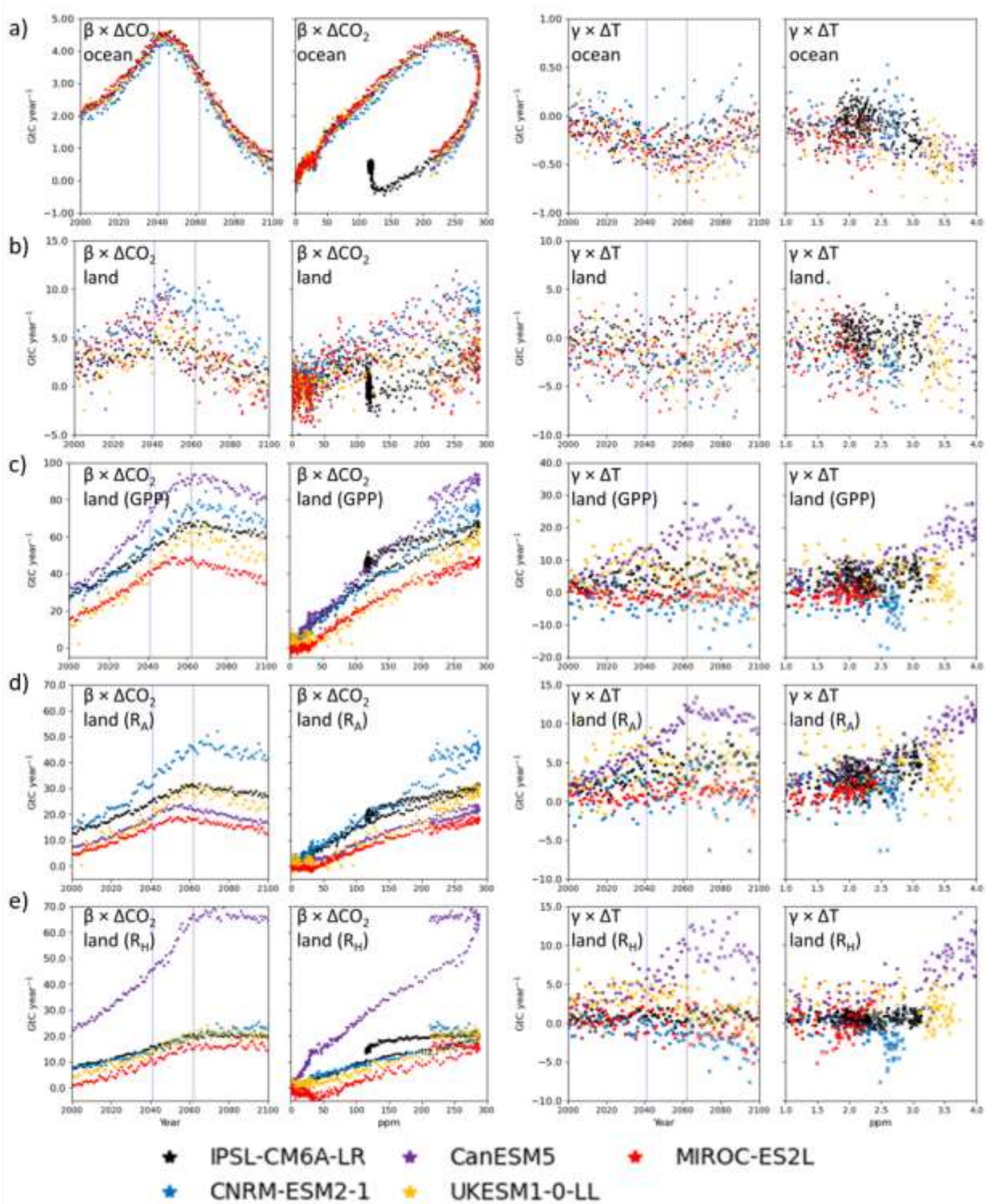

Figure 6. Breakdown of land and ocean carbon uptakes to the contributions of β and γ (GtC year^{-1}) as a function of time, CO_2 concentration, and temperature. Contributions are calculated as

yearly change of $\beta \times \Delta CO_2$ and $\gamma \times \Delta T$ for (a) ocean carbon uptake fgco2, (b) NBP, (c) GPP, (d) R_A and (e) R_H. The figures in the first column show β as a function of time (year) and in the second column as a function of CO_2 concentration (ppm). The figures in the third column show γ as a function of time (year) and in the fourth column as a function of temperature (°C). GPP, NBP, and fgco2 are positive to the surface, R_A and R_H are positive to the atmosphere. We use extended to 2300 data for IPSL-CM6A-LR. . In the first and third columns, the years of peak atmospheric CO_2 concentration and CO_2 growth rate are indicated by vertical black and blue dashed lines, respectively. The markers "*" and "×" indicate the periods before and after the peak of CO_2 concentration in 2062, respectively.

6 Conclusion

This study investigated the carbon cycle response of the six CMIP6 ESMs to the temperature overshoot under the SSP5-3.4-OS pathway. The land and ocean continue to remove carbon from the atmosphere at least for 50 years after the peak of the CO_2 growth rate. They only turn to a source afterward in the first half of the 22nd century for a short period and become a weak sink later, i.e., reach a new steady-state. From the perspective of the carbon cycle feedback framework, the land and ocean act as a carbon sink during both ramp-up and ramp-down stages of overshoot in the 21st century because the β carbon gain $\beta \times \Delta CO_2$ is large than γ loss $\gamma \times \Delta T$ under the considered pathway.

The decrease in the land and ocean uptakes occurs immediately after the start of mitigation efforts, and before the peaks of CO_2 concentration and temperature. The decrease in ocean uptake is driven by the dependency of the ocean sink on the CO_2 growth rate. Both land and ocean carbon uptakes show a strong nearly linear dependency on the CO_2 growth rate with the hysteresis behavior after the peak of the CO_2 increase.

The decrease in land uptake is driven by the net effect of the decreasing rate of GPP increase and the increase in TER due to delayed warming after CO_2 concentration change. Besides, land-use change emissions induced by the broad expansion of biofuel crops in SSP5-3.4-OS contribute to the early peak of land uptake. This finding suggests that the choice of negative emission approaches is important and may affect the overall global carbon uptake (Jones et al., 2010; 2016a).

Despite differences, CMIP6 ESMs agree on the amplification of the carbon cycle feedback parameters after the peaks of atmospheric CO_2 concentration and temperature due to the inertia of the Earth System. The ESMs show that β becomes more positive and γ more negative. The increase in feedback parameters after the peaks of CO_2 concentration and temperature reflects the decreasing yet persisting carbon uptake by the ocean and land during the ramp-down phase. Land and ocean continue to take up carbon (even though at a decreasing rate) at a rate larger than expected from linear behavior.

The amplification of carbon cycle feedback parameters influences the overall uptake by land and ocean under mitigation scenarios and thus affects the ability of the Earth System to return to the temperature target after an overshoot. We encourage future studies to investigate the consequences of amplification of feedback parameters under different overshoot pathways to understand what this means in the mitigation context.

Acknowledgments and Data

This work benefited from the scientific contributions of several researchers, in particular, Tomohiro Hajima of Japan Agency for Marine-Earth Science and Technology, Roland Séférian of CNRM, and Masakazu Yoshimori of The University of Tokyo. The data from the CMIP6 simulations are available from the CMIP6 archive (https://esgf-node.llnl.gov/search/cmip6). Data of GCB2019 are accessible via http://www.globalcarbonproject.org/carbonbudget, CarbonTracker2019 via http://carbontracker.noaa.gov CAMS via https://apps.ecmwf.int/datasets/data/cams-ghg-inversions/, the IIASA database via https://tntcat.iiasa.ac.at/SspDb/dsd?Action=htmlpage&page=welcome. This work was supported by a grant from the French Ministry of the Ecological Transition as part of the Convention on financial support for climate services, by The Ministry of Education, Culture, Sports, Science and Technology (MEXT) of Japan (Integrated Research Program for Advancing Climate Models, grant no. JPMXD0717935715) and the Environment Research and Technology Development Fund (JPMEERF20192004) of the Environmental Restoration and Conservation Agency of Japan. K. Tanaka benefited from State assistance managed by the National Research Agency in France under the “Programme d’Investissements d’Avenir” under the reference “ANR-19-MPGA-0008”. Study was also supported by the European Union’s Horizon 2020 research and innovation programme under grant agreement number 820829 for the "Constraining uncertainty of multi-decadal climate projections (CONSTRAIN)" project (07/2019-06/2024).

Author contributions

K. Tanaka conceived the research with input from O.B. and PCi. I.M. led the study, conducted the analysis, and generated all figures and tables. PCa and K.Tachiiri performed additional Earth system model simulations. I.M. and all co-authors discussed the results. I.M. drafted the manuscript, with input from all co-authors.

Conflict of Interest

The authors do not declare any competing interests.

References

Arora, V. K., Boer, G. J., Friedlingstein, P., Eby, M., Jones, C. D., Christian, J. R., et al. (2013). Carbon–Concentration and Carbon–Climate Feedbacks in CMIP5 Earth System Models. *Journal of Climate*, *26*(15), 5289–5314. https://doi.org/10.1175/JCLI-D-12-00494.1

Arora, V. K., Katavouta, A., Williams, R. G., Jones, C. D., Brovkin, V., Friedlingstein, P., et al. (2020). Carbon–concentration and carbon-climate feedbacks in CMIP6 models and their comparison to CMIP5 models. *Biogeosciences*, *17*(16), 4173–4222. https://doi.org/10.5194/bg-17-4173-2020

Boucher, O., Halloran, P. R., Burke, E. J., Doutriaux-Boucher, M., Jones, C. D., Lowe, J., et al. (2012). Reversibility in an Earth System model in response to CO_2 concentration changes. *Environmental Research Letters*, *7*(2), 024013. https://doi.org/10.1088/1748-9326/7/2/024013

Boucher, O., Servonnat, J., Albright, A. L., Aumont, O., Balkanski, Y., Bastrikov, V., et al. (2020). Presentation and Evaluation of the IPSL-CM6A-LR Climate Model. *Journal of Advances in Modeling Earth Systems*, *12*(7), e2019MS002010. https://doi.org/10.1029/2019MS002010

Chevallier, F. (2013). On the parallelization of atmospheric inversions of CO_2 surface fluxes within a variational framework. *Geoscientific Model Development*, *6*(3), 783–790. https://doi.org/10.5194/gmd-6-783-2013

Ciais, P., Yao, Y., Gasser, T., Baccini, A., Wang, Y., Lauerwald, R., et al. (2020). Empirical estimates of regional carbon budgets imply reduced global soil heterotrophic respiration. *National Science Review*. https://doi.org/10.1093/nsr/nwaa145

Danabasoglu, G., Lamarque, J.-F., Bacmeister, J., Bailey, D. A., DuVivier, A. K., Edwards, J., et al. (2020). The Community Earth System Model Version 2 (CESM2). *Journal of Advances in Modeling Earth Systems*, *12*(2), e2019MS001916. https://doi.org/10.1029/2019MS001916

Denvil-Sommer, A., Gehlen, M., Vrac, M., and Mejia, C. (2019) LSCE-FFNN-v1: a two-step neural network model for the reconstruction of surface ocean pCO2 over the global ocean, Geosci. Model Dev., 12, 2091–2105, https://doi.org/10.5194/gmd-12-2091-2019,

Eyring, V., Bony, S., Meehl, G. A., Senior, C. A., Stevens, B., Stouffer, R. J., & Taylor, K. E. (2016). Overview of the Coupled Model Intercomparison Project Phase 6 (CMIP6) experimental design and organization. *Geoscientific Model Development*, *9*(5), 1937. https://doi.org/10.5194/gmd-9-1937-2016

Friedlingstein, P., Cox, P., Betts, R., Bopp, L., von Bloh, W., Brovkin, V., Cadule, P., Doney, et al. (2006). Climate–Carbon Cycle Feedback Analysis: Results from the C4MIP Model Intercomparison. *Journal of Climate*, *19*(14), 3337–3353. https://doi.org/10.1175/JCLI3800.1

Friedlingstein, P., Jones, M. W., O'Sullivan, M., Andrew, R. M., Hauck, J., Peters, G. P., Peters, W., Pongratz, J., et al. (2019). Global Carbon Budget 2019. *Earth System Science Data*, *11*(4), 1783–1838. https://doi.org/10.5194/essd-11-1783-2019

Gasser, T., & Ciais, P. (2013). A theoretical framework for the net land-to-atmosphere CO_2 flux and its implications in the definition of "emissions from land-use change." *Earth System Dynamics*, *4*(1), 171–186. https://doi.org/10.5194/esd-4-171-2013

Gasser T., Kechiar M, Ciais P, Burke EJ, Kleinen T, Zhu D, Huang Y, Ekici A, et al. (2018). Path-dependent reductions in CO_2 emission budgets caused by permafrost carbon release. *Nature Geoscience* 11: 830-835. DOI:10.1038/s41561-018-0227-0

Gregory, J. M., Jones, C. D., Cadule, P., & Friedlingstein, P. (2009). Quantifying Carbon Cycle Feedbacks. *Journal of Climate*, *22*(19), 5232–5250. https://doi.org/10.1175/2009JCLI2949.1

Gruber, N., Clement, D., Carter, B. R., Feely, R. A., Heuven, S. van, Hoppema, M., et al. (2019). The oceanic sink for anthropogenic CO_2 from 1994 to 2007. *Science*, *363*(6432), 1193–1199. https://doi.org/10.1126/science.aau5153

Hajima, T., Watanabe, M., Yamamoto, A., Tatebe, H., Noguchi, M. A., Abe, M., Ohgaito, R., Ito, A., et al. (2020). Development of the MIROC-ES2L Earth system model and the evaluation of biogeochemical processes and feedbacks. *Geoscientific Model Development*, *13*(5), 2197–2244. https://doi.org/10.5194/gmd-13-2197-2020

Hausfather, Z., & Peters, G. P. (2020). Emissions – the 'business as usual' story is misleading. *Nature*, *577*(7792), 618–620. https://doi.org/10.1038/d41586-020-00177-3

Höhne, N., Elzen, M. den, Rogelj, J., Metz, B., Fransen, T., Kuramochi, T., Olhoff, A., Alcamo, J., et al. (2020). Emissions: world has four times the work or one-third of the time. *Nature*, *579*(7797), 25–28. https://doi.org/10.1038/d41586-020-00571-x

Huntzinger, D. N., Michalak, A. M., Schwalm, C., Ciais, P., King, A. W., Fang, Y., Schaefer, K., Wei, Y., et al. (2017). Uncertainty in the response of terrestrial carbon sink to environmental drivers undermines carbon-climate feedback predictions. *Scientific Reports*, *7*(1), 4765. https://doi.org/10.1038/s41598-017-03818-2

Hurtt, G. C., Chini, L., Sahajpal, R., Frolking, S., Bodirsky, B. L., Calvin, K., Doelman, J.C., Fisk, J., et al. (2020). Harmonization of Global Land-Use Change and Management for the Period 850–2100 (LUH2) for CMIP6. *Geoscientific Model Development Discussions*, 1–65. https://doi.org/10.5194/gmd-2019-360

Jacobson, A. R., Schuldt, K. N., Miller, J. B., Oda, T., Tans, P., Andrews, A., Mund, J., Ott, L., et al. (2020). CarbonTracker CT2019. https://doi.org/10.25925/39M3-6069

Jeltsch-Thömmes, A., Stocker, T. F., & Joos, F. (2020). Hysteresis of the Earth system under positive and negative CO_2 emissions. *Environmental Research Letters*. https://doi.org/10.1088/1748-9326/abc4af doi:https://doi.org/10.22033/ESGF/CMIP6.6401

Jones, C. D., Arora, V., Friedlingstein, P., Bopp, L., Brovkin, V., Dunne, J., Graven, H., Hoffman, F., et al. (2016b). C4MIP – The Coupled Climate–Carbon Cycle Model Intercomparison Project: experimental protocol for CMIP6. *Geoscientific Model Development*, *9*(8), 2853–2880. https://doi.org/10.5194/gmd-9-2853-2016

IPCC (Intergov. Panel Clim. Change). (2018). Global Warming of 1.5° C. An IPCC Special Report on the Impacts of Global Warming of 1.5° C Above Pre-Industrial Levels and Related Global Greenhouse Gas Emission Pathways, in the Context of Strengthening the Global Response to the Threat of Climate Change, Sustainable Development, and Efforts to Eradicate Poverty.

Jones, C.D., Ciais, P., Davis, S.J., Friedlingstein, P., Gasser, T., Peters, G.P., Rogelj, J., van Vuuren D.P., et al. (2016a). Simulating the Earth system response to negative emissions. Environmental Research Letters, 11(9), 095012.

Jones, C. D., & Friedlingstein, P. (2020). Quantifying process-level uncertainty contributions to TCRE and carbon budgets for meeting Paris Agreement climate targets. *Environmental Research Letters*, *15*(7), 074019. https://doi.org/10.1088/1748-9326/ab858a

Jones, C. D, Liddicoat, S. & Lowe, J. (2010) Role of terrestrial ecosystems in determining CO2 stabilization and recovery behaviour, Tellus B: Chemical and Physical Meteorology, 62:5, 682-699, DOI: 10.1111/j.1600-0889.2010.00490.x

Khatiwala, S., Primeau, F., & Hall, T. (2009). Reconstruction of the history of anthropogenic CO 2 concentrations in the ocean. *Nature*, *462*(7271), 346–349. https://doi.org/10.1038/nature08526

Landschützer, P., Gruber, N., and Bakker, D. C. E. (2016) Decadal variations and trends of the global ocean carbon sink, *Global Biogeochem. Cy.*, 30, 1396–1417, https://doi.org/10.1002/2015GB005359

Koven, C. D., Chambers, J. Q., Georgiou, K., Knox, R., Negron-Juarez, R., Riley, W. J., et al. (2015). Controls on terrestrial carbon feedbacks by productivity versus turnover in the CMIP5 Earth System Models. Biogeosciences, 12(17), 5211–5228. https://doi.org/10.5194/bg-12-5211-2015

Mallapaty, S. (2020). How China could be carbon neutral by mid-century. *Nature, 586*(7830), 482–483. https://doi.org/10.1038/d41586-020-02927-9

Meinshausen, M., Nicholls, Z. R. J., Lewis, J., Gidden, M. J., Vogel, E., Freund, M., Beyerle, U., Gessner, C., et al. (2020). The shared socio-economic pathway (SSP) greenhouse gas concentrations and their extensions to 2500. *Geoscientific Model Development*, *13*(8), 3571–3605. https://doi.org/10.5194/gmd-13-3571-2020

Meinshausen, M., E. Vogel, A. Nauels, K. Lorbacher, N. Meinshausen, D. Etheridge, P. Fraser, S.A. Montzka, et al. (2016), Historical greenhouse gas concentrations, doi:10.5194/gmd-2016-169

McKinley, G. A., Fay, A. R., Eddebbar, Y. A., Gloege, L., & Lovenduski, N. S. (2020). External forcing explains recent decadal variability of the ocean carbon sink. *AGU Advances*, 1, e2019AV000149. https://doi.org/10.1029/2019AV000149

O'Neill, B. C., Kriegler, E., Riahi, K., Ebi, K. L., Hallegatte, S., Carter, T. R., Mathur, R. & van Vuuren, D.P., (2014). A new scenario framework for climate change research: the concept of shared socioeconomic pathways. *Climatic Change*, *122*(3), 387–400. https://doi.org/10.1007/s10584-013-0905-2

O'Neill, B. C., Kriegler, E., Ebi, K. L., Kemp-Benedict, E., Riahi, K., Rothman, D. S., van Ruijven, B.J., van Vuuren, D.P., et al. (2017). The roads ahead: Narratives for shared socioeconomic pathways describing world futures in the 21st century. *Global Environmental Change, 42*, 169–180. https://doi.org/10.1016/j.gloenvcha.2015.01.004

Palter, J. B., Frölicher, T. L., Paynter, D., & John, J. G. (2018). Climate, ocean circulation, and sea level changes under stabilization and overshoot pathways to 1.5 K warming. *Earth System Dynamics*, *9*(2), 817–828. https://doi.org/10.5194/esd-9-817-2018

Rödenbeck, C., Bakker, D. C. E., Metzl, N., Olsen, A., Sabine, C., Cassar, N., Reum, F., Keeling, R. F., & Heimann, M. (2014) Interannual sea–air CO_2 flux variability from an observation-driven ocean mixed-layer scheme, *Biogeosciences*, 11, 4599-4613.

Schwalm, C. R., Glendon, S., & Duffy, P. B. (2020). RCP8.5 tracks cumulative CO_2 emissions. *Proceedings of the National Academy of Sciences*, *117*(33), 19656–19657. https://doi.org/10.1073/pnas.2007117117

Schwinger, J., & Tjiputra, J. (2018). Ocean Carbon Cycle Feedbacks Under Negative Emissions. *Geophysical Research Letters*, *45*(10), 5062–5070. https://doi.org/10.1029/2018GL077790

Séférian, R., Nabat, P., Michou, M., Saint-Martin, D., Voldoire, A., Colin, J., Decharme, B., Delire, C., et al. (2019). Evaluation of CNRM Earth System Model, CNRM-ESM2-1: Role of Earth System Processes in Present-Day and Future Climate. *Journal of Advances in Modeling Earth Systems*, *11*(12), 4182–4227. https://doi.org/10.1029/2019MS001791 doi:https://doi.org/10.22033/ESGF/CMIP6.4223

Séférian, R., Berthet, S., Yool, A., Palmiéri, J., Bopp, L., Tagliabue, A., Kwiatkowski, L., Aumont, O., et al. (2020). Tracking Improvement in Simulated Marine Biogeochemistry Between CMIP5 and CMIP6. *Current Climate Change Reports*, *6*(3), 95–119. https://doi.org/10.1007/s40641-020-00160-0

Séférian, R., Nabat, P., Michou, M., Saint-Martin, D., Voldoire, A., Colin, J., Decharme, B., Delire, C., et al. 2019. Evaluation of CNRM Earth System Model, CNRM-ESM2-1: Role of Earth System Processes in Present-Day and Future Climate. *Journal of Advances in Modeling Earth Systems*, 11(12), pp.4182-4227. https://doi.org/10.1029/2019MS001791

Sellar, A. A., Jones, C. G., Mulcahy, J. P., Tang, Y., Yool, A., Wiltshire, A., O'connor, F.M., Stringer, M., et al. (2019). UKESM1: Description and Evaluation of the U.K. Earth System Model. *Journal of Advances in Modeling Earth Systems*, *11*(12), 4513–4558. https://doi.org/10.1029/2019MS001739

Swart, N.C., Cole, J.N., Kharin, V.V., Lazare, M., Scinocca, J.F., Gillett, N.P., Anstey, J., Arora, et al. (2019a). The Canadian Earth System Model version 5 (CanESM5.0.3). *Geoscientific Model Development*, *12*(11), 4823–4873. https://doi.org/10.5194/gmd-12-4823-2019

Tachiiri, K. (2020). Relationship between physical and biogeochemical parameters and the scenario dependence of the transient climate response to cumulative carbon emissions. Progress in Earth and Planetary Science, 7(1), 74. https://doi.org/10.1186/s40645-020-00392-6

Tebaldi, C., Debeire, K., Eyring, V., Fischer, E., Fyfe, J., Friedlingstein, P., Knutti, R., Lowe, J., et al.: Climate model projections from the Scenario Model Intercomparison Project (ScenarioMIP) of CMIP6, *Earth Syst. Dynam. Discuss.*, https://doi.org/10.5194/esd-2020-68, in review, 2020.

Tokarska, K. B., Zickfeld, K., & Rogelj, J. (2019). Path Independence of Carbon Budgets When Meeting a Stringent Global Mean Temperature Target After an Overshoot. *Earth's Future*, *7*(12), 1283–1295. https://doi.org/10.1029/2019EF001312

United Nations / Framework Convention on Climate Change (2015). FCCC/CP/2015/L.9/Rev.1: Adoption of the Paris Agreement, (pp. 1–32). UNFCCC, Paris, France.

Williams, R.G., Katavouta, A. & Goodwin, P. Carbon-Cycle Feedbacks Operating in the Climate System. Curr Clim Change Rep 5, 282–295 (2019). https://doi.org/10.1007/s40641-019-00144-9

Willeit, M., Ganopolski, A., Dalmonech, D., Foley, A. M., & Feulner, G. (2014). Time-scale and state dependence of the carbon-cycle feedback to climate. *Climate dynamics*, 42(7-8), 1699-1713.

Zickfeld, K., MacDougall, A. H., & Matthews, H. D. (2016). On the proportionality between global temperature change and cumulative CO_2 emissions during periods of net negative CO_2 emissions. *Environmental Research Letters*, *11*(5), 055006. https://doi.org/10.1088/1748-9326/11/5/055006

Earth's Future

Supporting Information for

Carbon cycle response to temperature overshoot beyond 2 °C – an analysis of CMIP6 models

I. Melnikova[1,2], O. Boucher[1], P. Cadule[1], P. Ciais[3], T. Gasser[4], Y. Quilcaille[4], H. Shiogama[2], K. Tachiiri[2,5], T. Yokohata[2] and K. Tanaka[2,3]

[1] Institut Pierre-Simon Laplace, Sorbonne Université / CNRS, France

[2] Center for Global Environmental Research (CGER), National Institute for Environmental Studies (NIES), Japan

[3] Laboratoire des Sciences du Climat et de l'Environnement (LSCE), Commissariat à l'énergie atomique et aux énergies alternatives (CEA CNRS UVSQ), Gif-sur-Yvette, France

[4] International Institute for Applied Systems Analysis (IIASA), Austria

[5] Research Institute for Global Change, Japan Agency for Marine-Earth Science and Technology, Japan

Contents of this file

Table S1 and figures S1 to S15

Introduction

This supporting information contains a table and fifteen figures.

Table S1. Ensemble members used in each experiment and each model

ESM	IPSL-CM6A-LR	CNRM-ESM2-1	CanESM5	MIROC-ES2L	UKESM1-0-LL	CESM2-WACCM
piControl	r1i1p1f1	r1i1p1f2	r1i1p1f1, r1i1p2f1	r1i1p1f2	r1i1p1f2 (parent to r4..)	r1i1p1f1
historical	r1i1p1f1 (1910)	r1i1p1f2 (1850)	r1i1p1f1 (5201)	r1i1p1f2 (1850)	r4i1p1f2 (1960)	r1i1p1f1 (55)
ssp534-over	r1i1p1f1	r1i1p1f2	r1i1p1f1	r1i1p1f2	r4i1p1f2	r1i1p1f1
ssp585	r1i1p1f1	r1i1p1f2	r1i1p1f1	r1i1p1f2	r4i1p1f2	r1i1p1f1
hist-bgc	r1i1p1f1 (1910)	r1i1p1f2 (1850)	r1i1p2f1 (5550)	r1i1p1f2 (1850)	r4i1p1f2 (1960)	
ssp534-over-bgc	r1i1p1f1	r1i1p1f2	r1i1p2f1	r1i1p1f2	r4i1p1f2	
ssp585-bgc	r1i1p1f1	r1i1p1f2	r1i1p2f1	r1i1p1f2	r4i1p1f2	

Values in the bracket indicate the branching year from the piControl.

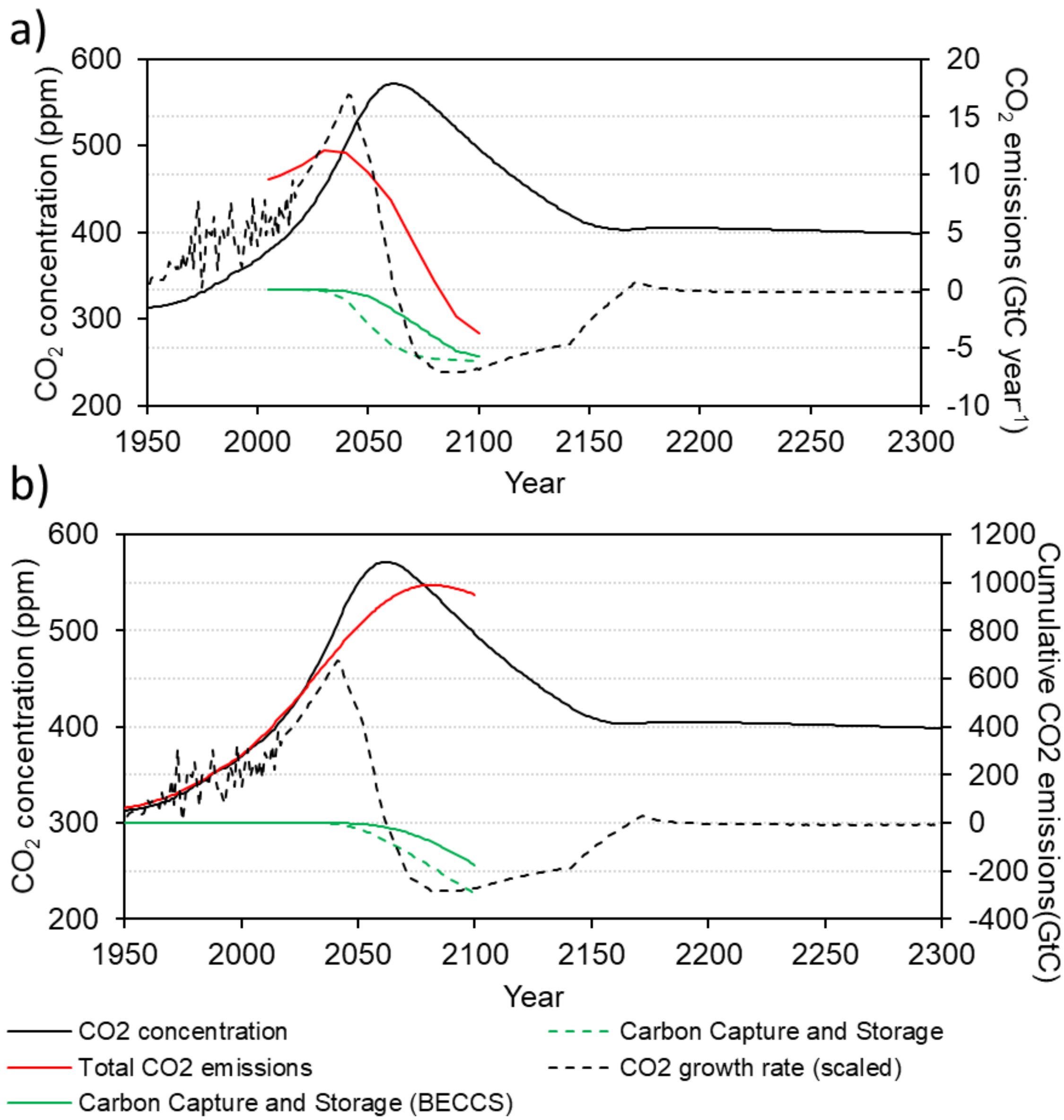

Figure S1. Time series of CO_2 concentration (ppm), CO_2 growth rate (scaled) and corresponding (a) CO_2 emissions (GtC $year^{-1}$) and (b) cumulative CO_2 emissions (GtC) by REMIND-MAgPIE from input4MIP for SSP-5-3.4-OS experiment. Emission data are from the Integrated Assessment Modeling Consortium & International Institute for Applied Systems Analysis (IIASA) database at https://tntcat.iiasa.ac.at/SspDb/dsd?Action=htmlpage&page=welcome. Fossil fuel emission data prior year 2005 are from the GCB2019 data set.

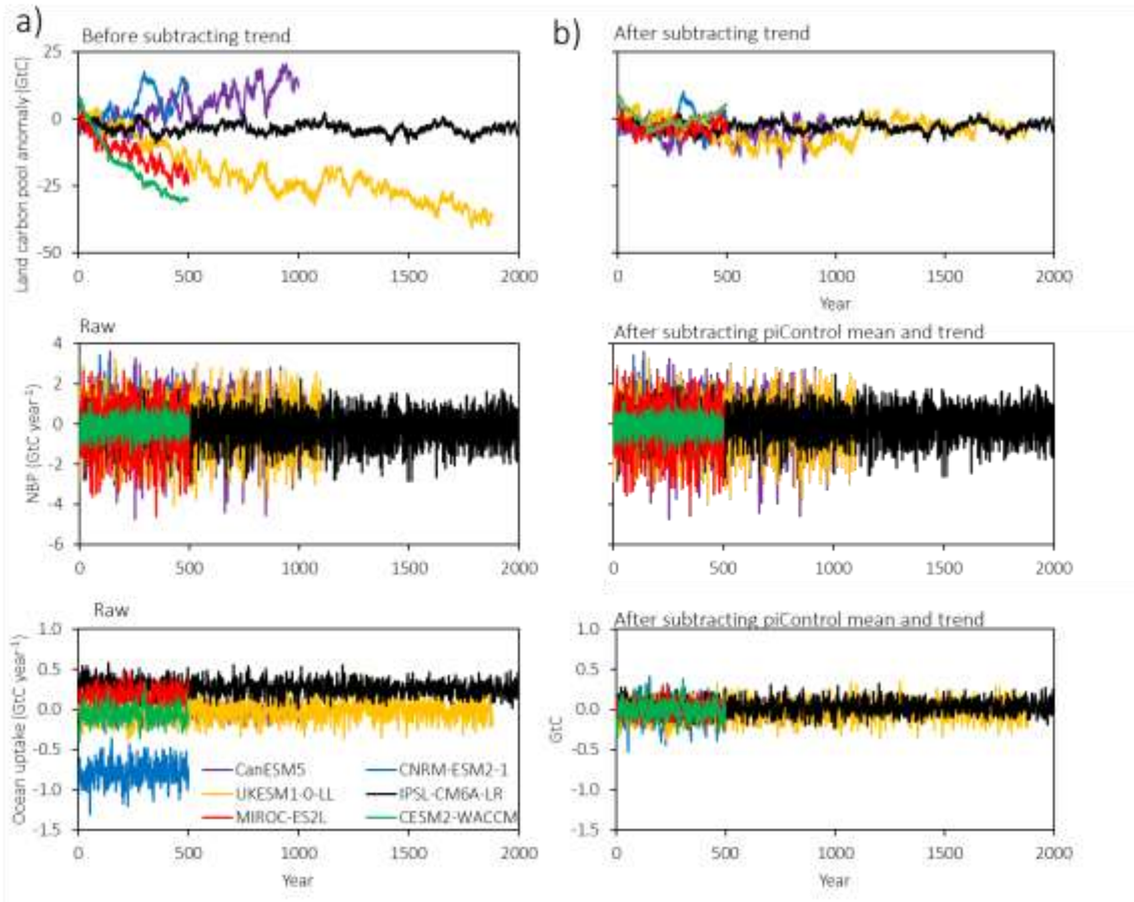

Figure S2. Time series of changes in global land biomass, land (NBP), and ocean carbon uptakes in the piControl experiment before (a) and after (b) pre-processing.

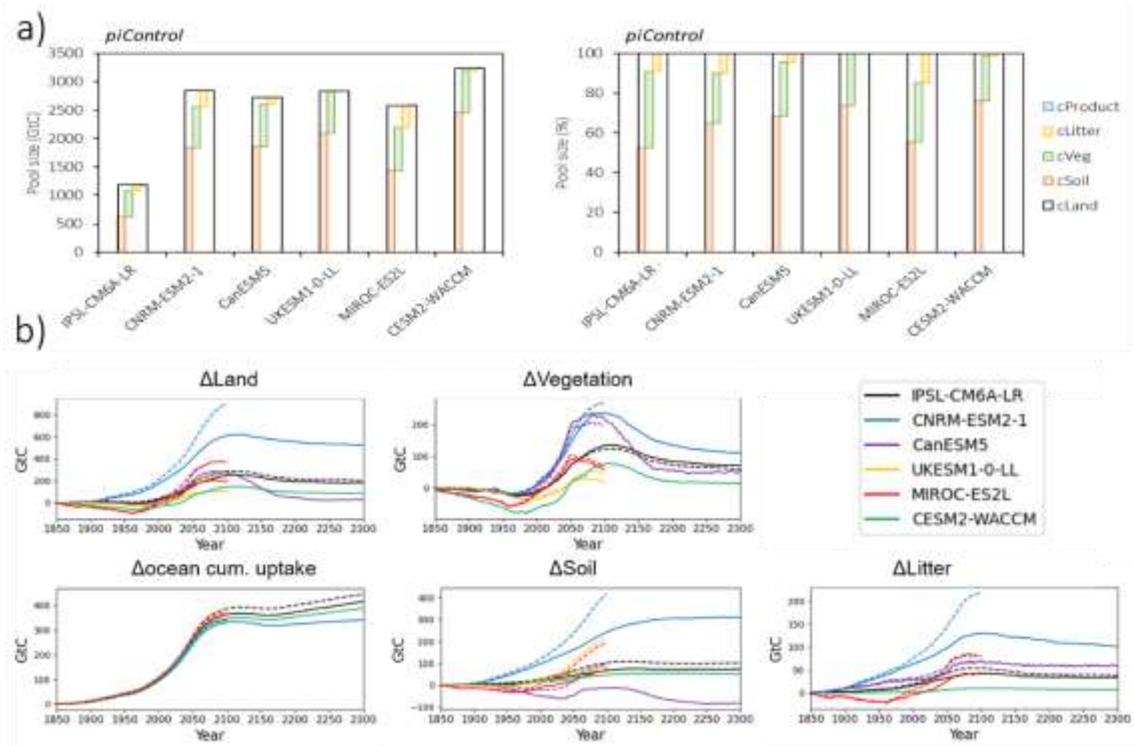

Figure S3. Mean land carbon pool sizes in piControl by six earth system models in fully and biogeochemically coupled simulations of SSP5-3.4-OS experiment (a). Time series of land carbon pools and cumulative ocean flux anomalies from piControl (b). Solid lines indicate COU run, and dashed lines indicate BGC run.

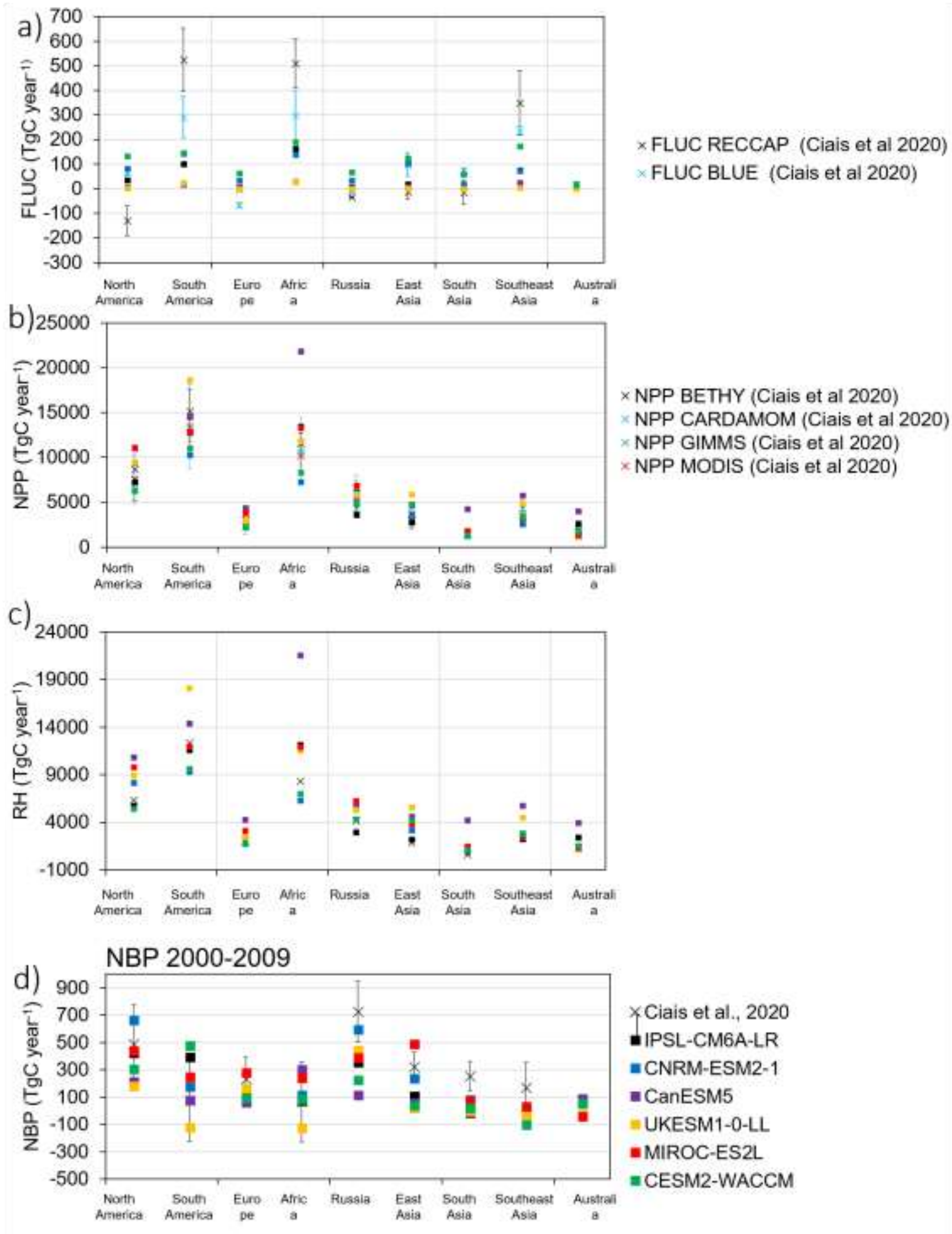

Figure S4. An evaluation of Earth system models (ESMs) against observational data set by Ciais et al. (2020). (a) fLUC, (b) NPP, (c) R_H, and (d) NBP absolute value with associated uncertainty at nine RECCAP regions in 2000-2009.

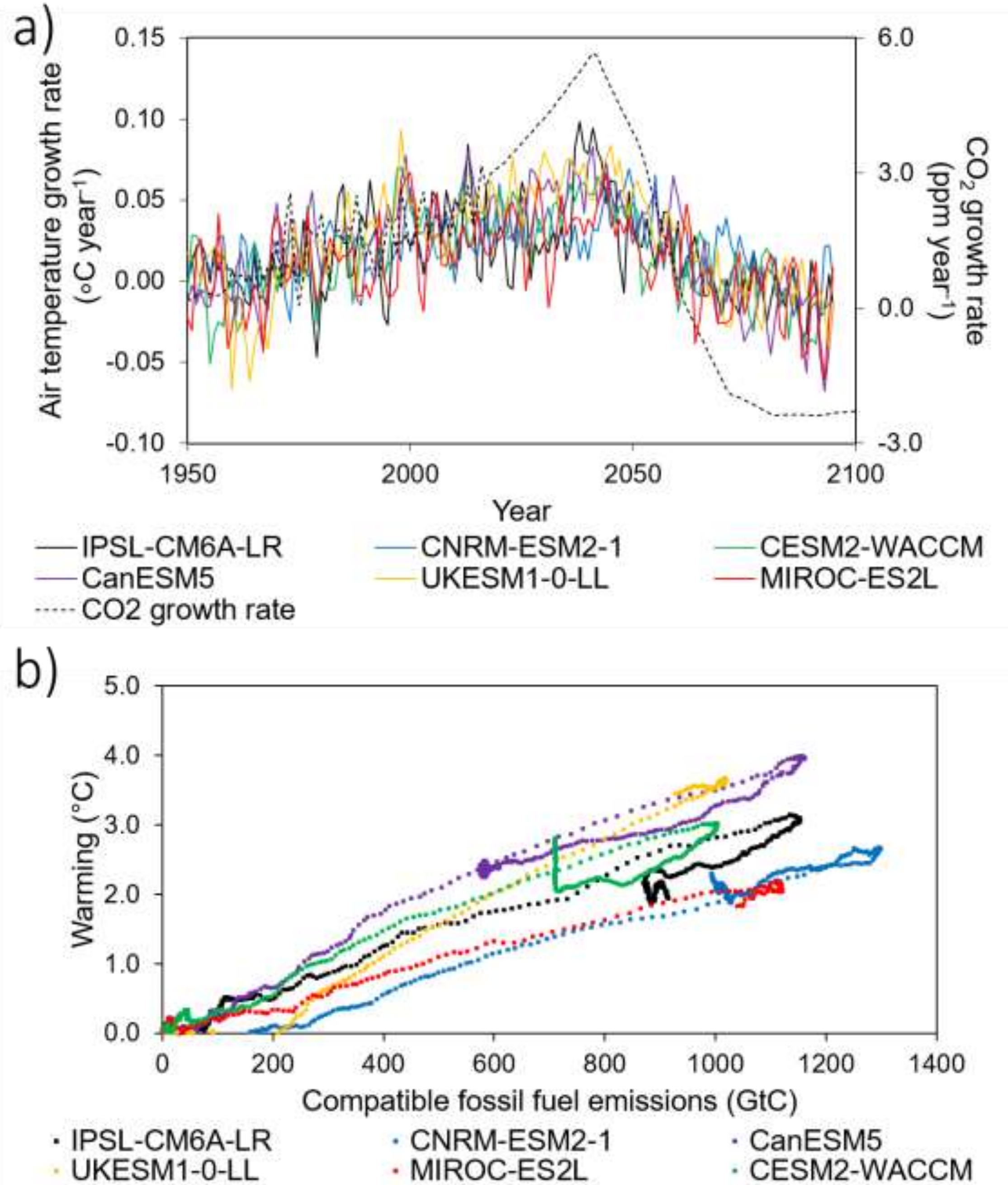

Figure S5. Time series of the growth rate of air temperature and by six earth system models and CO_2 concentration in SSP5-3.4-OS experiment (a). Rates of change in air temperature are given as a 10-year moving average. The surface air temperature changes relative to 1850–1999 mean versus cumulative compatible fossil fuel emissions in the SSP5-3.4-OS pathway (b). The slope of the curves is the transient climate response to cumulative emissions (TCRE).

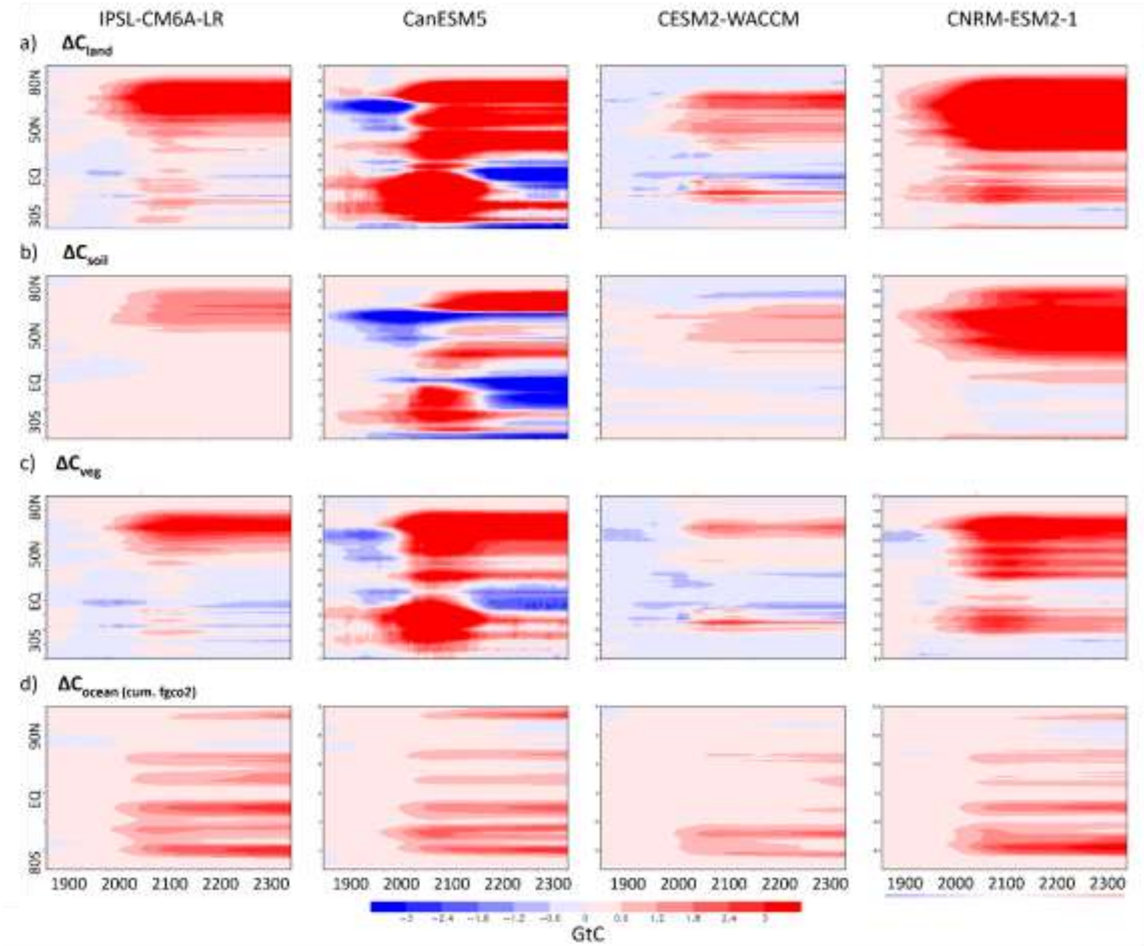

Figure S6. The spatiotemporal variation of zonal cumulative (a) ΔC_{land}, (b) ΔC_{soil}, (c) $\Delta C_{soil,}$ and ΔC_{ocean} (GtC) in 1900-2300 under SSP5-3.4-OS pathway. ΔC_{ocean} is calculated from cumulative flux fgco2 over time.

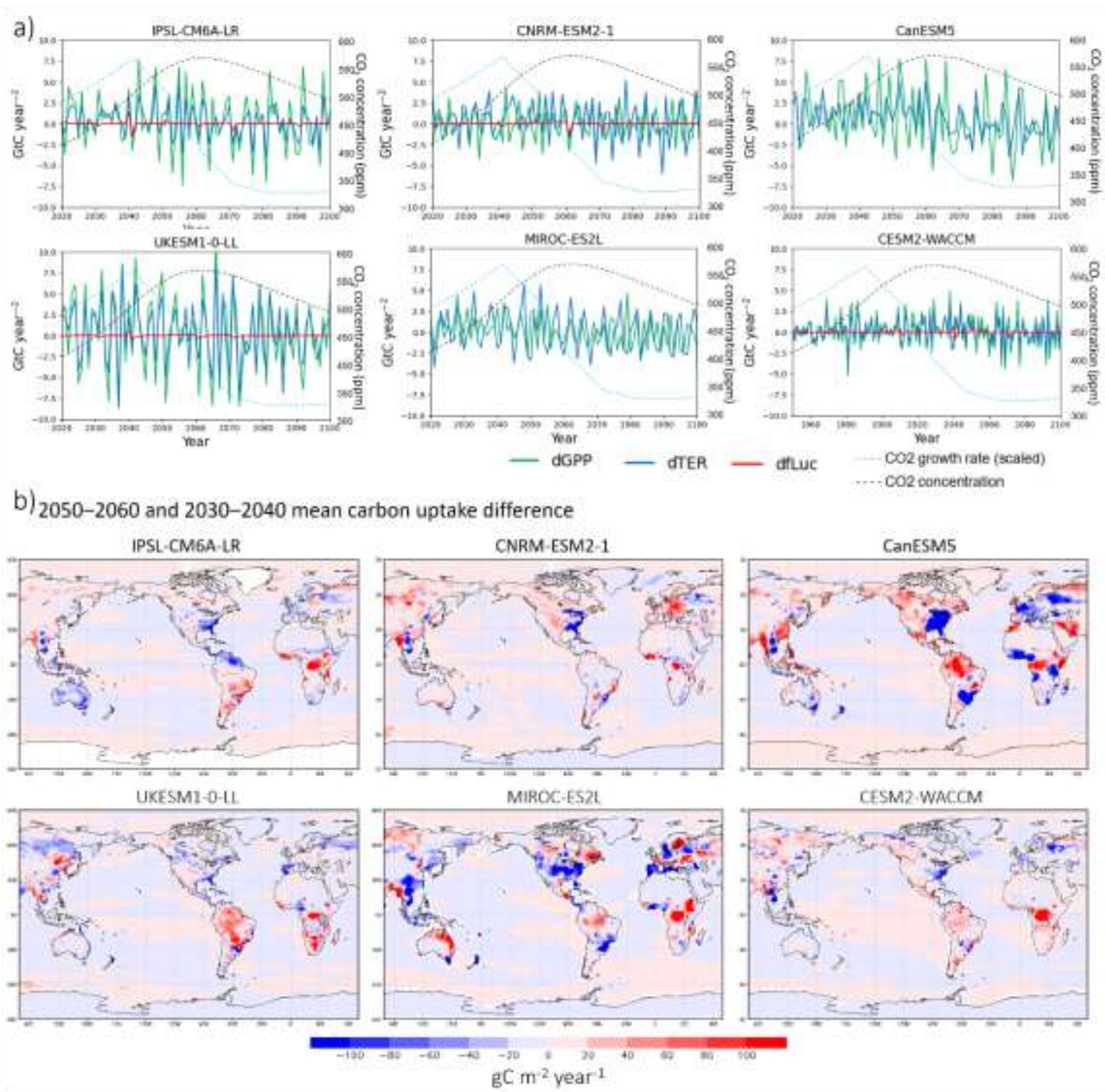

Figure S7. Panel (a) shows the time series of the derivatives of GPP, TER, fLUC (GtC year^{-2}), CO2 concentration (ppm), and scaled CO2 growth rate. fLUC is missing in CanESM5 and MIROC-ES2L because model teams did not provide this variable. Panel (b) shows the spatial variation of the difference between the mean ocean and land uptakes (NBP and fgco2) in 2050–2060 and 2030–2040. Positive values indicate an increase in carbon uptake in a later period.

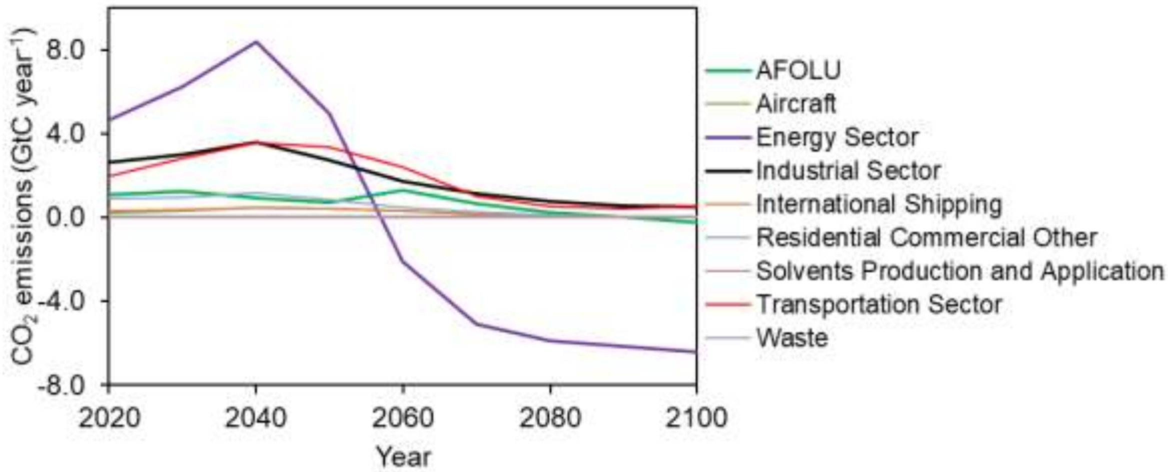

Figure S8. Time series of changes in CO_2 emissions simulated by REMIND-MAGPIE under SSP5-3.4-OS pathway.

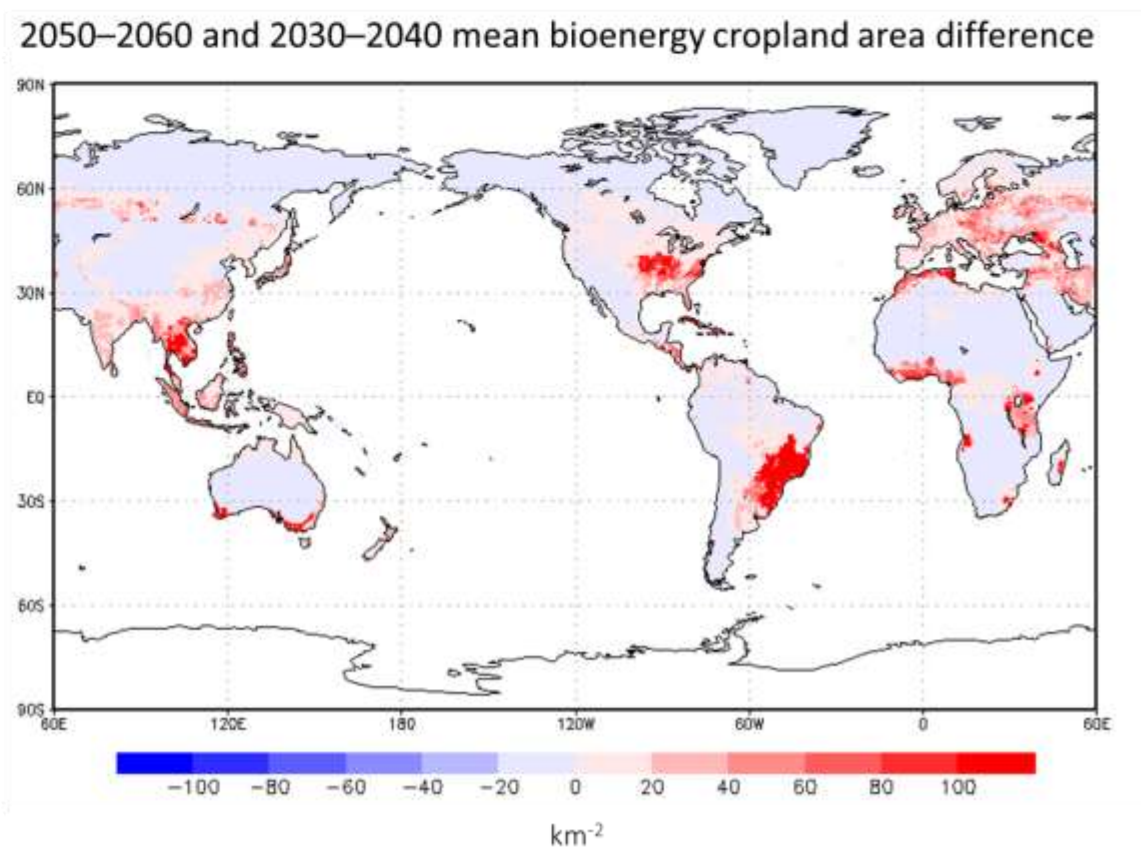

Figure S9. Difference between the mean bioenergy cropland area in 2050–2060 and 2030–2040 based on the LUH2 data set.

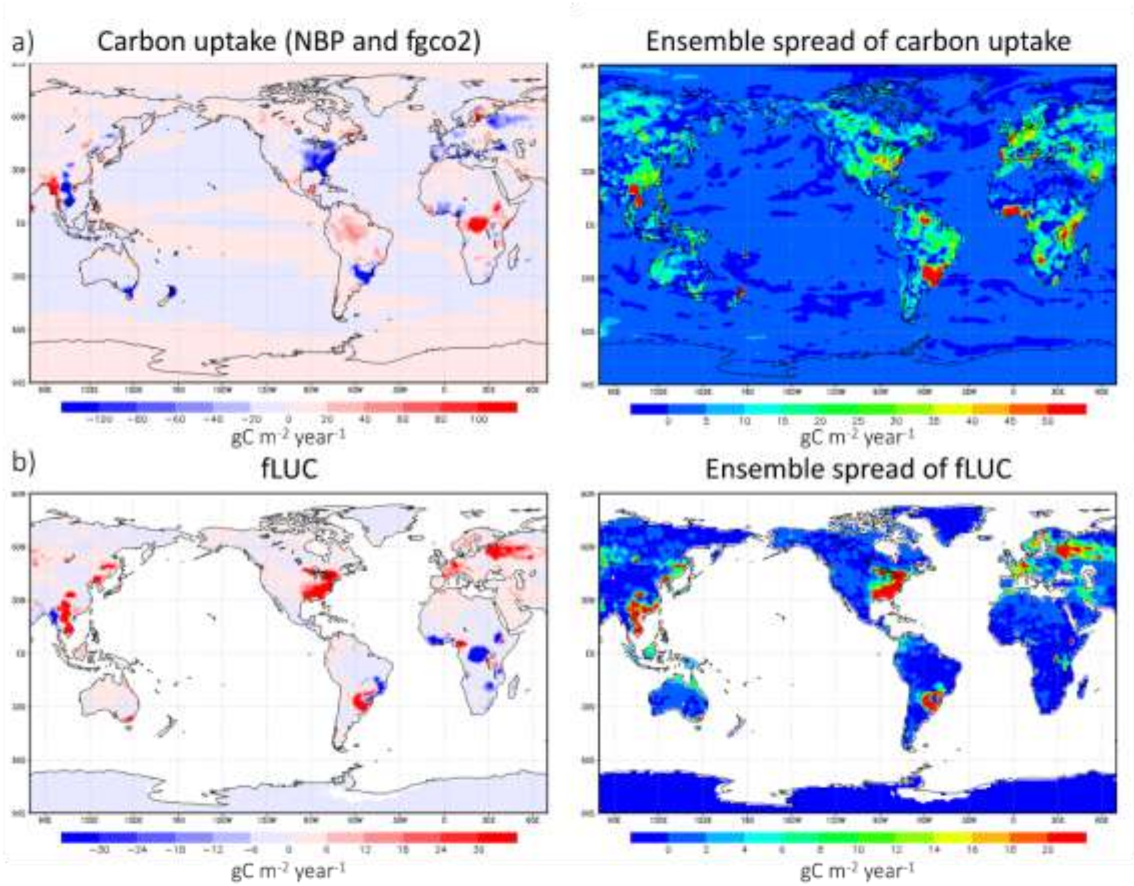

Figure S10. The difference in (a) the carbon uptake and (b) land-use change emissions before and after the peak of CO_2 concentration is shown as ensemble means of six (four for fLUC) CMIP6 ESMs.

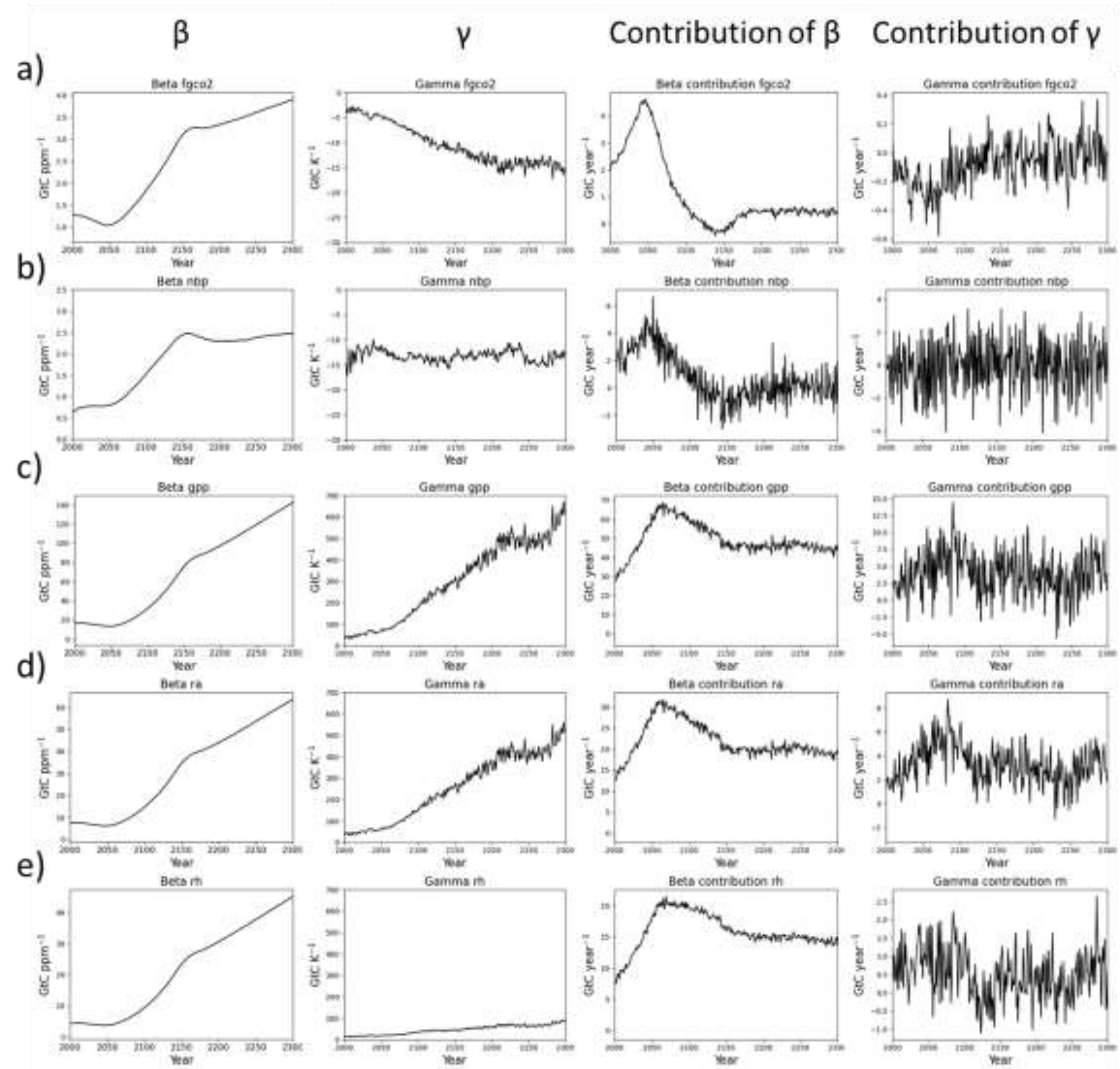

Figure S11. Carbon-concentration β (GtC ppm^{-1}), carbon-temperature γ (GtC °C^{-1}) feedback parameters and their contributions to the carbon fluxes (GtC year^{-1}) for (a) ocean fgco2, and land (b) NBP, (c) GPP, (d) R_A and (e) R_H as a function of time (year) extended till the year 2300 for IPSL-CM6A-LR under the SSP5-3.4-OS pathway.

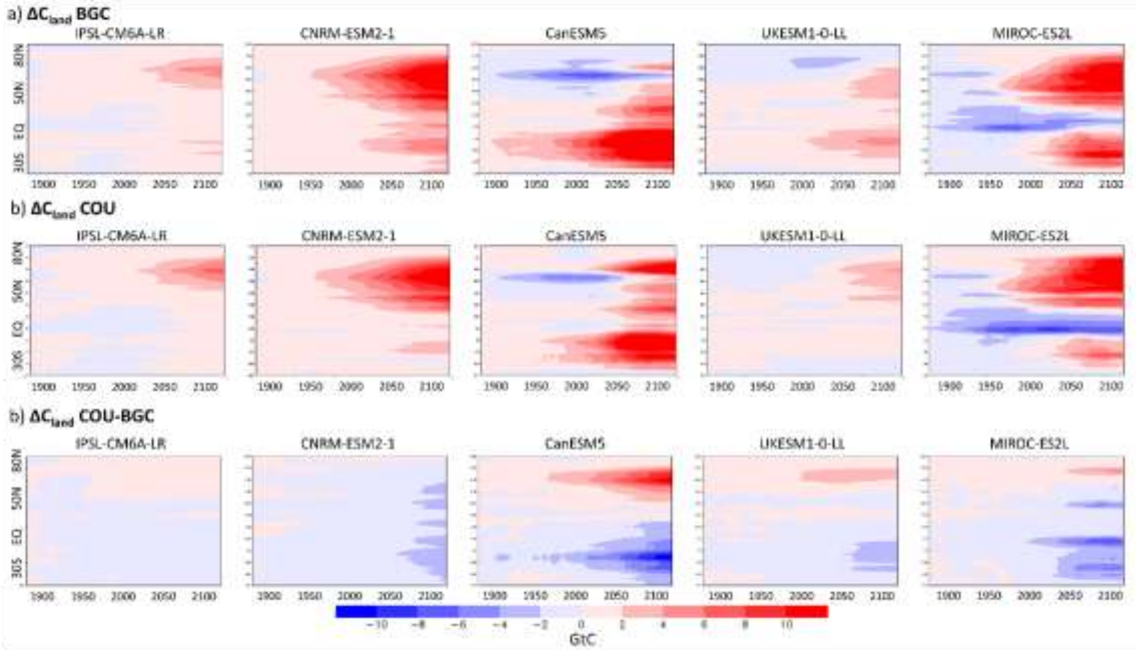

Figure S12. The spatiotemporal variation of zonal cumulative land carbon pool (positive to land) in (a) BGC simulation, (b) COU simulation, and (c) COU-BGC difference.

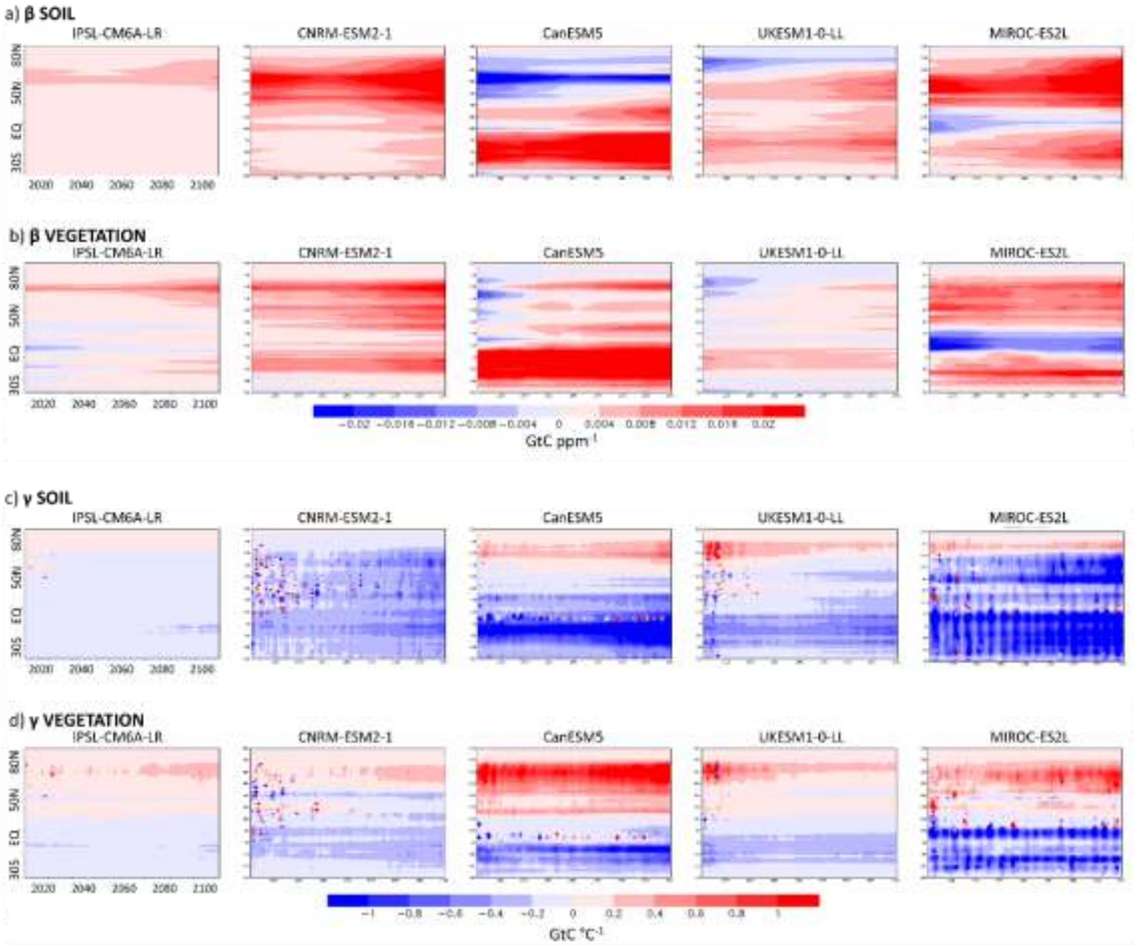

Figure S13. The spatiotemporal variation of zonal cumulative (a) β_{soil}, (b) β_{veg} (GtC ppm-1), (c) γ_{soil} and (d) γ_{veg} (GtC °C^{-1}) calculated from corresponding land carbon pools. Positive values indicate a net sink.

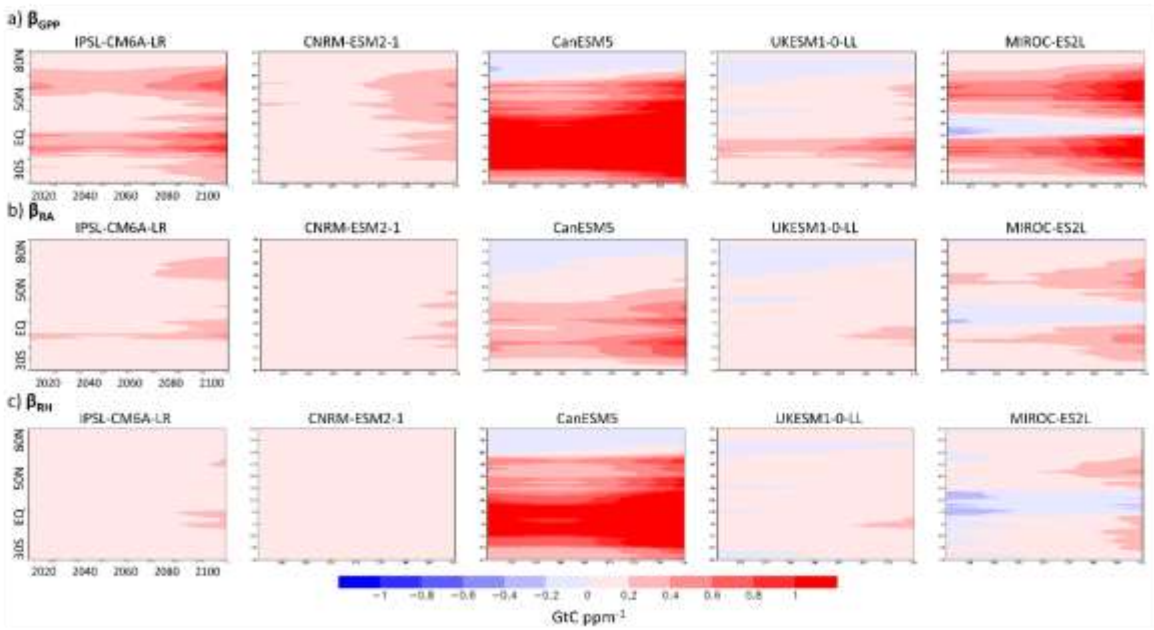

Figure S14. The spatiotemporal variation of zonal cumulative (a) β_{GPP}, (b) $\beta_{RA,}$ and (c) β_{RH} (GtC ppm^{-1}) is calculated from corresponding cumulative land carbon fluxes. Positive values indicate a net sink for β_{GPP} and a net source for β_{RA} and β_{RH}.

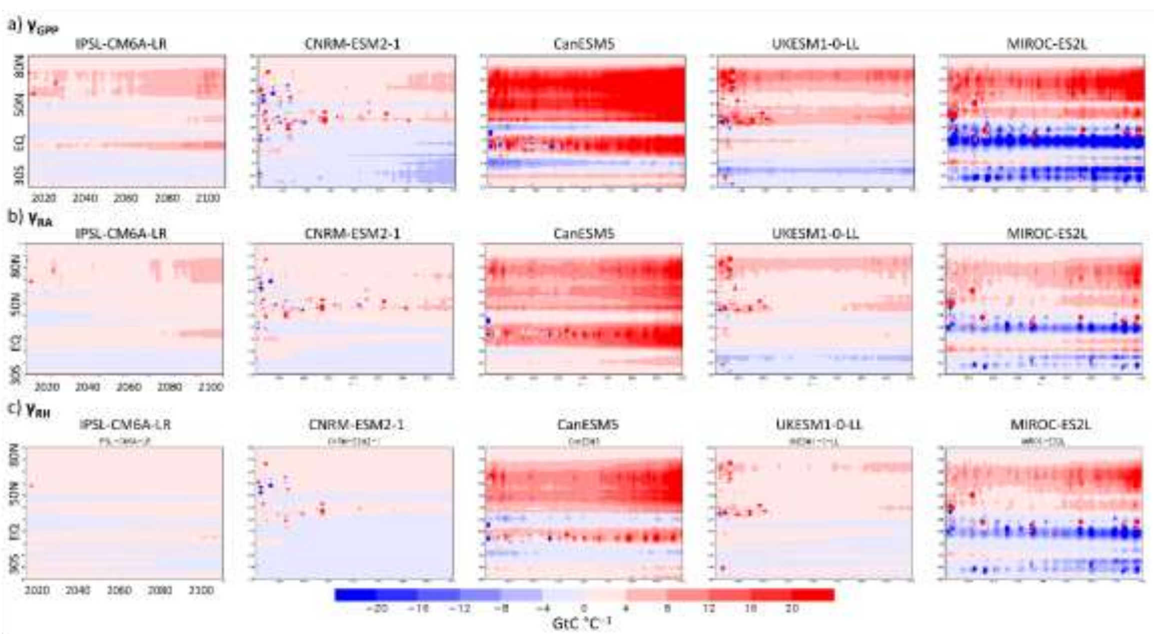

Figure S15. The spatiotemporal variation of zonal cumulative (a) γ_{GPP}, (b) γ_{RA}, and (c) γ_{RH} (GtC °C $^{-1}$) calculated from corresponding cumulative land carbon fluxes. Positive values indicate a net sink for γ_{GPP} and a net source for γ_{RA} and γ_{RH}.